Article

Astrocytic interleukin-3 programs microglia and limits Alzheimer's disease

Cameron S. McAlpine[1,2,3], Joseph Park[4], Ana Griciuc[4], Eunhee Kim[4], Se Hoon Choi[4], Yoshiko Iwamoto[1], Máté G. Kiss[1], Kathleen A. Christie[5], Claudio Vinegoni[1], Wolfram C. Poller[1,2], John E. Mindur[1], Christopher T. Chan[1], Shun He[1], Henrike Janssen[1], Lai Ping Wong[6,7], Jeffrey Downey[1], Sumnima Singh[1], Atsushi Anzai[1], Florian Kahles[1], Mehdi Jorfi[4], Paolo Fumene Feruglio[8], Ruslan I. Sadreyev[6,9], Ralph Weissleder[1], Benjamin P. Kleinstiver[5], Matthias Nahrendorf[1], Rudolph E. Tanzi[4 ✉] & Filip K. Swirski[1,2 ✉]

Communication within the glial cell ecosystem is essential for neuronal and brain health[1-3]. The influence of glial cells on the accumulation and clearance of β-amyloid (Aβ) and neurofibrillary tau in the brains of individuals with Alzheimer's disease (AD) is poorly understood, despite growing awareness that these are therapeutically important interactions[4,5]. Here we show, in humans and mice, that astrocyte-sourced interleukin-3 (IL-3) programs microglia to ameliorate the pathology of AD. Upon recognition of Aβ deposits, microglia increase their expression of IL-3Rα—the specific receptor for IL-3 (also known as CD123)—making them responsive to IL-3. Astrocytes constitutively produce IL-3, which elicits transcriptional, morphological, and functional programming of microglia to endow them with an acute immune response program, enhanced motility, and the capacity to cluster and clear aggregates of Aβ and tau. These changes restrict AD pathology and cognitive decline. Our findings identify IL-3 as a key mediator of astrocyte–microglia cross-talk and a node for therapeutic intervention in AD.

The role of glial cell communication in the pathophysiology of AD remains poorly defined[2,3]. IL-3 is a multifunctional cytokine that has been implicated in inflammatory and autoimmune diseases[6]. In humans, IL-3 levels are associated with risk[7-10] and severity[11,12] of AD, and in vitro studies have implicated IL-3 in neurodegeneration[13-16]. Despite these links, the role of IL-3 in the brains of humans with AD or in mouse models of AD is not well understood.

First, we profiled the brains of wild-type and IL-3-deficient (Il3^{−/−}) mice. In otherwise healthy mice, IL-3 deficiency did not affect blood–brain barrier permeability, neurogenesis, neuronal death, microglia activation and proliferation, or performance on a Y-maze task (Extended Data Fig. 1). To test the function of IL-3 in AD, we crossed Il3^{−/−} mice with 5xFAD mice (a mouse model of AD in which five familial AD-associated mutations are expressed) and found increased Aβ aggregates, Aβ plaque size, and Aβ levels in the cortex of Il3^{−/−} 5xFAD mice (Fig. 1a–c). The Il3^{−/−} 5xFAD mice demonstrated impaired short-term (Fig. 1d) and spatial learning memory (Fig. 1e, Extended Data Fig. 2a), and showed a tendency towards reduced memory retention (Fig. 1f). These observations suggest that IL-3 has a protective role in a mouse model of AD.

Because IL-3 governs haematopoiesis[6], we assessed leukocyte generation. Compared to wild-type mice, 5xFAD mice had more

haematopoietic progenitor cells in the bone marrow and more circulating myeloid cells (Extended Data Fig. 2b, c). Deletion of Il3 had modest effects on haematopoiesis in 5xFAD mice. Despite these findings, we did not observe altered blood–brain barrier permeability (Extended Data Fig. 2d) or seeding of the brain parenchyma by peripheral leukocytes in 5xFAD or Il3^{−/−} 5xFAD mice (Extended Data Fig. 2e, f), suggesting that blood-derived leukocytes are rare in the brains of 5xFAD mice, regardless of IL-3 levels. Although these data do not exclude the possibility that vascular skull channels[17] or the meninges[18] are sources of immune cells[19,20], they propose that IL-3 functions in the local brain environment.

We measured IL-3 levels in plasma and the cerebrospinal fluid (CSF). The levels were similar in wild-type and 5xFAD mice, but IL-3 concentration was fourfold higher in the CSF than in the plasma, which suggests that IL-3 may be generated locally in the brain (Fig. 2a). To test this possibility, we designed a CRISPR–Cas9-based editing strategy to generate dual Il3 reporter/floxed mice (Il3[GFPfl/fl] mice; Supplementary Tables 1–5, Extended Data Fig. 3a–d). We confirmed successful sequence insertion and GFP signal in CD4^{+} T cells, a known IL-3 source[21] (Extended Data Fig. 3e). Notably, flow cytometry of whole brain tissue from Il3[GFPfl/fl] mice revealed that about 4% of astrocytes, but not microglia or other CD45^{−} cells, produced IL-3 (Fig. 2b, Extended Data Fig. 4a, b). Evaluation of Il3[GFPfl/fl] 5xFAD mice suggested that AD pathology does not appear to

[1]Center for Systems Biology and Department of Radiology, Massachusetts General Hospital and Harvard Medical School, Boston, MA, USA. [2]Cardiovascular Research Institute and Department of Medicine, Icahn School of Medicine at Mount Sinai, New York, NY, USA. [3]Friedman Brain Institute and Nash Family Department of Neuroscience, Icahn School of Medicine at Mount Sinai, New York, NY, USA. [4]Genetics and Aging Research Unit, McCance Center for Brain Health, Mass General Institute for Neurodegenerative Disease, Department of Neurology, Massachusetts General Hospital and Harvard Medical School, Charlestown, MA, USA. [5]Center for Genomic Medicine, Department of Pathology, Massachusetts General Hospital and Harvard Medical School, Boston, MA, USA. [6]Department of Molecular Biology, Massachusetts General Hospital, Boston, MA, USA. [7]Department of Genetics, Harvard Medical School, Boston, MA, USA. [8]Department of Neuroscience, Biomedicine and Movement Sciences, University of Verona, Verona, Italy. [9]Department of Pathology, Massachusetts General Hospital and Harvard Medical School, Boston, MA, USA. ✉e-mail: rtanzi@mgh.harvard.edu; filip.swirski@mssm.edu
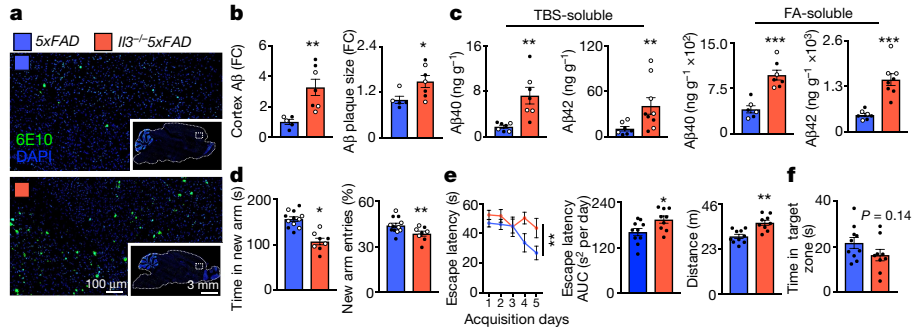
Fig. 1 | IL-3 protects against Aβ accumulation and cognitive impairment in 5xFAD mice. a, Representative images of Aβ in 5-month-old *5xFAD* and *Il3⁻/⁻5xFAD* mice. **b**, Quantification of Aβ area and Aβ plaque size in the cortex (*n* = 5 *5xFAD* mice; *n* = 7 *Il3⁻/⁻5xFAD* mice). **c**, Levels of tris-buffered saline (TBS)- and formic acid (FA)-soluble Aβ40 and Aβ42 in cortex homogenates from *5xFAD* and *Il3⁻/⁻5xFAD* mice (*n* = 7 *5xFAD* mice for TBS-soluble Aβ40 and Aβ42, FA-soluble Aβ42, *n* = 6 *5xFAD* mice for FA-soluble Aβ40; *n* = 7 *Il3⁻/⁻5xFAD* mice for TBS- and FA-soluble Aβ40, *n* = 9 *Il3⁻/⁻5xFAD* mice for TBS-soluble Aβ42, *n* = 8 *Il3⁻/⁻5xFAD* mice for FA-soluble Aβ42). **d**, Quantification of time in new arm and entries made into the new arm in a Y-maze (*n* = 12 *5xFAD* mice; *n* = 8 *Il3⁻/⁻5xFAD* mice). **e**, Time for male mice to reach hidden platform in Morris water maze plotted across training days (two-way ANOVA for groups, *P* = 0.0074), area under the curve (AUC) of escape latency and distance travelled (*n* = 10 *5xFAD* mice; *n* = 9 *Il3⁻/⁻5xFAD* mice). **f**, Time in target zone of Morris water maze on probe day (eighth day; *n* = 10 *5xFAD* mice; *n* = 9 *Il3⁻/⁻5xFAD* mice). Filled circles, male mice; open circles, female mice; mean ± s.e.m. **P* < 0.05, ***P* < 0.01, ****P* < 0.001; two-tailed Mann–Whitney *U*-tests unless otherwise indicated.
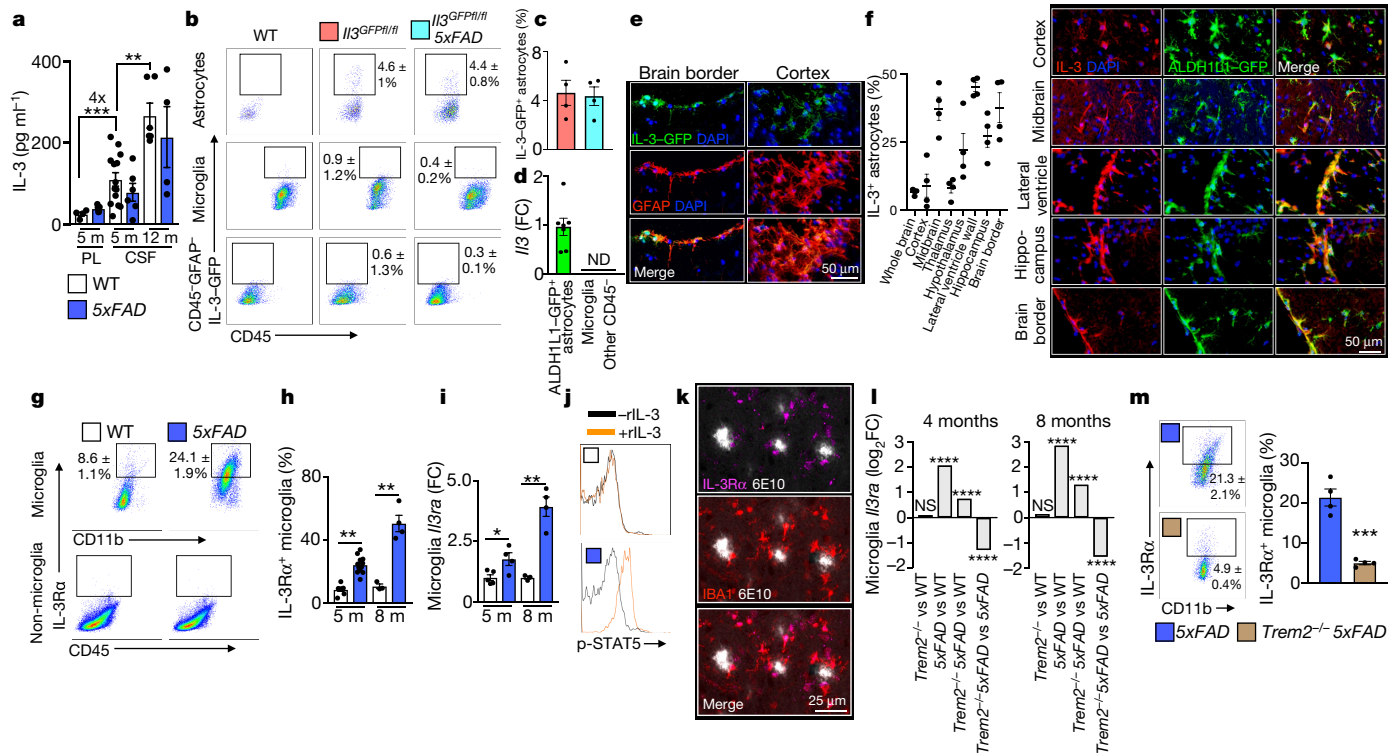

Fig. 2 | Microglia become responsive to astrocyte-derived IL-3 in AD. a, IL-3 in plasma (PL) and CSF of wild-type (WT) and *5xFAD* mice at 5 and 12 months (m) of age (*n* = 4 WT 5-m plasma; *n* = 5 *5xFAD* 5-m plasma; *n* = 14 WT 5-m CSF; *n* = 6 *5xFAD* 5-m CSF; *n* = 6 WT 12-m CSF; *n* = 4 *5xFAD* 12-m CSF). One-way ANOVA, multiple comparisons. 4×, fourfold increase. **b**, Flow cytometry analysis of brains from WT, *Il3^GFPfl/fl*, and *Il3^GFPfl/fl5xFAD* mice. **c**, Quantification of IL-3⁺ (GFP⁺) astrocytes in the brains of *Il3^GFPfl/fl* and *Il3^GFPfl/fl5xFAD* mice (*n* = 4). **d**, *Il3* expression in ALDH1L1–GFP⁺CD45⁻ astrocytes, CD11b⁺CD45^mid microglia, and CD45⁻ cells from *Aldh1l1^GFP* mice (*n* = 7). ND, not detected. **e**, Representative images showing co-localization of IL-3–GFP⁺ with GFAP⁺ astrocytes in *Il3^GFPfl/fl* mice. **f**, Quantification of IL-3⁺ astrocytes and representative images showing co-localization of IL-3 with GFP⁺ astrocytes in *Aldh1l1^GFP* mice (*n* = 4). **g**, **h**, Flow cytometry (**g**) and quantification (**h**) of IL-3Rα⁺ microglia in WT and *5xFAD* mice (*n* = 8 WT 5-m mice; *n* = 12 *5xFAD* 5-m mice; *n* = 3 WT 8-m mice; *n* = 4 *5xFAD* 8-m mice). One-way ANOVA, multiple comparisons. **i**, *Il3ra* in microglia (*n* = 5 WT 5-m mice; *n* = 4 *5xFAD* 5-m and 8-m mice; *n* = 3 WT 8-m mice). One-way ANOVA, multiple comparisons. **j**, p-STAT5 in ex vivo microglia with or without rIL-3. **k**, Representative images showing co-localization of IL-3Rα and IBA1 in proximity to Aβ in *5xFAD* mice. **l**, *Il3ra* in microglia from WT, *Trem2⁻/⁻*, *5xFAD*, and *Trem2⁻/⁻5xFAD* mice (for 4-month-old mice *P* = 3.45 × 10⁻²⁷ for *5xFAD* versus WT, *P* = 3.4 × 10⁻⁶ for *Trem2⁻/⁻5xFAD* versus WT, *P* = 1.82 × 10⁻⁸ for *Trem2⁻/⁻5xFAD* versus *5xFAD*; for 8-month-old mice *P* = 1.12 × 10⁻⁹³ for *5xFAD* versus WT, *P* = 1.4 × 10⁻¹³ for *Trem2⁻/⁻5xFAD* versus WT, *P* = 1.6 × 10⁻⁴⁰ for *Trem2⁻/⁻5xFAD* versus *5xFAD*; FDR < 0.0002; for WT *n* = 13 male (M)/14 female (F) at 4 m, *n* = 8M/8F at 8 m; for *Trem2⁻/⁻* *n* = 11M/12F at 4 m, 2M/2F at 8 m; for *5xFAD* *n* = 14M/14F at 4 m, 10M/9F at 8 m; for *Trem2⁻/⁻5xFAD* *n* = 11M/11F at 4 m, 9M/8F at 8 m). NS, not significant. One-way ANOVA. **m**, IL-3Rα⁺ microglia from *5xFAD* and *Trem2⁻/⁻5xFAD* mice (*n* = 4). Two-tailed Mann–Whitney *U*-test. Groups are of evenly mixed sex. **P* < 0.05, ***P* < 0.01, ****P* < 0.001. Mean ± s.e.m.
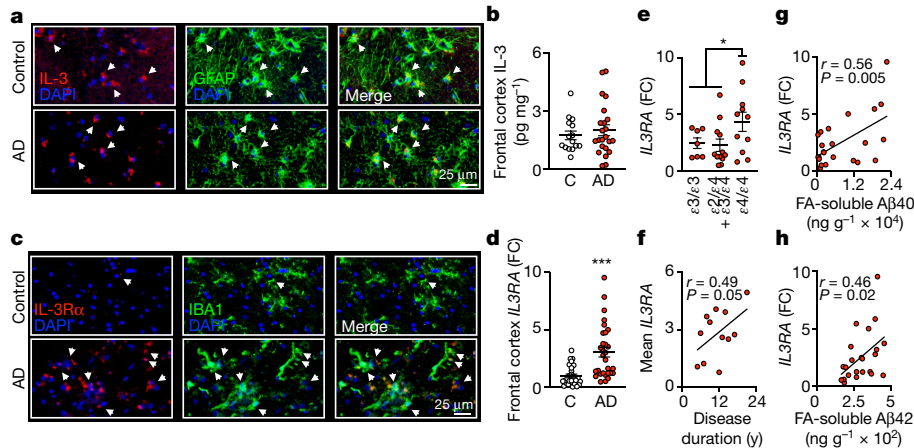
Fig. 3 | IL-3 signalling correlates with disease pathology in the brains of humans with AD. a, Representative images of the cortices of control donors (C) and individuals with AD stained for IL-3 and GFAP. **b**, IL-3 levels in cortex tissue homogenates from control donors and individuals with AD ($n = 15$ C, $n = 23$ AD; Extended Data Table 1). Two-tailed Mann–Whitney U-test. **c**, Representative images of the cortices of control donors (C) and individuals with AD stained for IL-3Rα and IBA1. **d**, Quantitative PCR (qPCR) analysis of *IL3RA* expression in the frontal cortices of control donors (C) and individuals

with AD ($n = 28$ C, $n = 30$ AD; Extended Data Table 1). Two-tailed Mann–Whitney U-test. **e**, Brain *IL3RA* expression according to *APOE* genotype in patients with AD ($n = 30$). One-way ANOVA, multiple comparisons. **f**, Correlation of mean *IL3RA* expression with years of AD duration ($n = 30$). Pearson's correlation. **g**, **h**, Correlation of *IL3RA* expression with FA-soluble Aβ40 (**g**) and Aβ42 (**h**) in frontal cortex from patients with AD ($n = 23$). Pearson's correlation. *$P < 0.05$, **$P < 0.01$, ***$P < 0.001$. Mean ± s.e.m.

change IL-3 production by astrocytes (Fig. 2b, c). *Il3* expression was specific to astrocytes (Fig. 2d, Extended Data Fig. 4c), age-dependent, and comparable between wild-type and *5xFAD* mice (Extended Data Fig. 5a). Imaging of *Il3*GFPfl/fl mice showed co-localization of GFP with GFAP+ astrocytes (Fig. 2e), strengthening the idea that a subset of astrocytes is the primary source of IL-3 in the mouse brain.

To investigate region-specific heterogeneity in the production of IL-3 by astrocytes, we profiled astrocyte reporter (*Aldh1l1*GFP) mice. IL-3 was co-localized with ALDH1L1–GFP+ astrocytes, but not with ALDH1L1–GFP− cells (non-astrocytes) (Fig. 2f, Extended Data Fig. 4e). The proportion of IL-3+ astrocytes varied across brain structures (Fig. 2f). However, owing to the function of IL-3 as a secreted cytokine and its presence in the circulating CSF, tissue IL-3 levels were comparable throughout the brain (Extended Data Fig. 5b). Activation of astrocytes did not modify IL-3 production (Extended Data Fig. 5c, d) and *Il3* deletion did not alter the morphology or distribution of astrocytes in healthy or *5xFAD* mice (Extended Data Fig. 5e, f). These results suggest that a subset of astrocytes constitutively generates IL-3.

We sought to identify the brain cells that respond to IL-3 and identified an age-dependent increase in IL-3Rα in the microglia of wild-type mice (Extended Data Fig. 5g, h). Microglia in *5xFAD* mice showed elevated IL-3Rα at a much earlier age (Fig. 2g–i, Extended Data Fig. 4d). In 5- and 8-month-old *5xFAD* mice, IL-3Rα+ microglia constituted more than 20% and 50% of the microglial pool, respectively. By contrast, in wild-type mice IL-3Rα+ microglia accounted for about 8% of cells at these ages. Premature IL-3Rα augmentation in *5xFAD* mice was specific to microglia and did not occur in other brain cell types (Fig. 2g) or in peripheral macrophages (Extended Data Fig. 5i). We confirmed robust IL-3Rα signalling in microglia from *5xFAD* but not wild-type mice (Fig. 2j), and found that IL-3Rα co-localized with microglia in close proximity to Aβ aggregates (Fig. 2k). These results indicate that microglia become responsive to IL-3 during AD by expressing IL-3Rα.

To explore networks that control dynamic *Il3ra* expression, we profiled microglia from wild-type, *Trem2*−/−, *5xFAD*, and *Trem2*−/−*5xFAD* mice by RNA sequencing (RNA-seq). TREM2 is an immune receptor that shapes the transcriptional and functional landscape of microglia[22–24]. We confirmed that *Il3ra* mRNA was enriched in microglia from *5xFAD* mice relative to wild-type mice at 4 months (log₂[fold-change

(FC)] = 2.068, $P = 3.45 \times 10^{-27}$) and 8 months (log₂FC = 2.851, $P = 1.12 \times 10^{-93}$) of age (Fig. 2l). We also noted an age-dependent increase in *Il3ra* (8- versus 4-month-old *5xFAD* mice; log₂FC = 0.758, $P = 5.49 \times 10^{-6}$). Notably, deletion of *Trem2* blunted *Il3ra* expression in *5xFAD* mice at 4 months (log₂FC = −1.288, $P = 1.82 \times 10^{-8}$) and 8 months (log₂FC = −1.552, $P = 1.60 \times 10^{-40}$) of age. Flow cytometry confirmed that *Trem2* deletion reduced the appearance of IL-3Rα+ microglia (Fig. 2m).

TREM2 mediates the development of disease-associated microglia (DAMs)—microglia with an activated and protective phenotype that occur with AD[22,23]. Analysis of public single-cell RNA-seq datasets[23] demonstrated that *Il3ra* is augmented in TREM2-dependent stage 2 DAMs, but not TREM2-independent stage 1 DAMs or homeostatic microglia (Extended Data Fig. 6a). To investigate whether IL-3Rα+ microglia represent a phenotypically unique sub-population, we profiled IL-3Rαhi and IL-3Rαlo microglia in the brains of *5xFAD* mice (Extended Data Fig. 6b–d). Consistent with the hypothesis that TREM2 is required for IL-3Rα induction, IL-3Rαhi microglia had higher levels of TREM2 and increased expression of the TREM2 adaptor protein DAP12 (*Tyrobp*) than IL-3Rαlo microglia. IL-3Rαhi microglia also exhibited increased levels of MHCII, CD11C (encoded by *Itgax*), CCL2, and intracellular Aβ, and higher expression of *Ccl2*, *Ccl7*, and *Ccl5*. These findings propose that IL-3Rα+ microglia are a distinct TREM2-dependent population endowed with an immune-responsive and activated phenotype.

Next, we assessed IL-3 signalling in the human brain (cohort characteristics in Extended Data Table 1). Histological analysis of post-mortem frontal cortex samples from patients with AD and age-matched control donors without dementia showed that IL-3 co-localized with astrocytes (Fig. 3a). Measurements of IL-3 in frontal cortex tissue homogenates indicated that IL-3 levels were unaltered by AD pathology (Fig. 3b). Meanwhile, microglia in the frontal cortex of healthy control donors exhibited numerous thin ramifications, suggestive of a resting state, and were devoid of IL-3Rα (Fig. 3c). By contrast, microglia in samples from patients with AD stained for IL-3Rα abundantly and had a globular and amoeboid morphology, which indicates microglial activation. Furthermore, there was a threefold increase in *IL3R*A expression in the brains of individuals with AD (Fig. 3d), and donors carrying the AD-risk *APOE*ε4/ε4 genotype showed higher *IL3R*A expression than did carriers of other *APOE* genotypes (Fig. 3e). *IL3R*A expression correlated with disease duration (Fig. 3f) and Aβ levels in donors with AD (Fig. 3g, h).
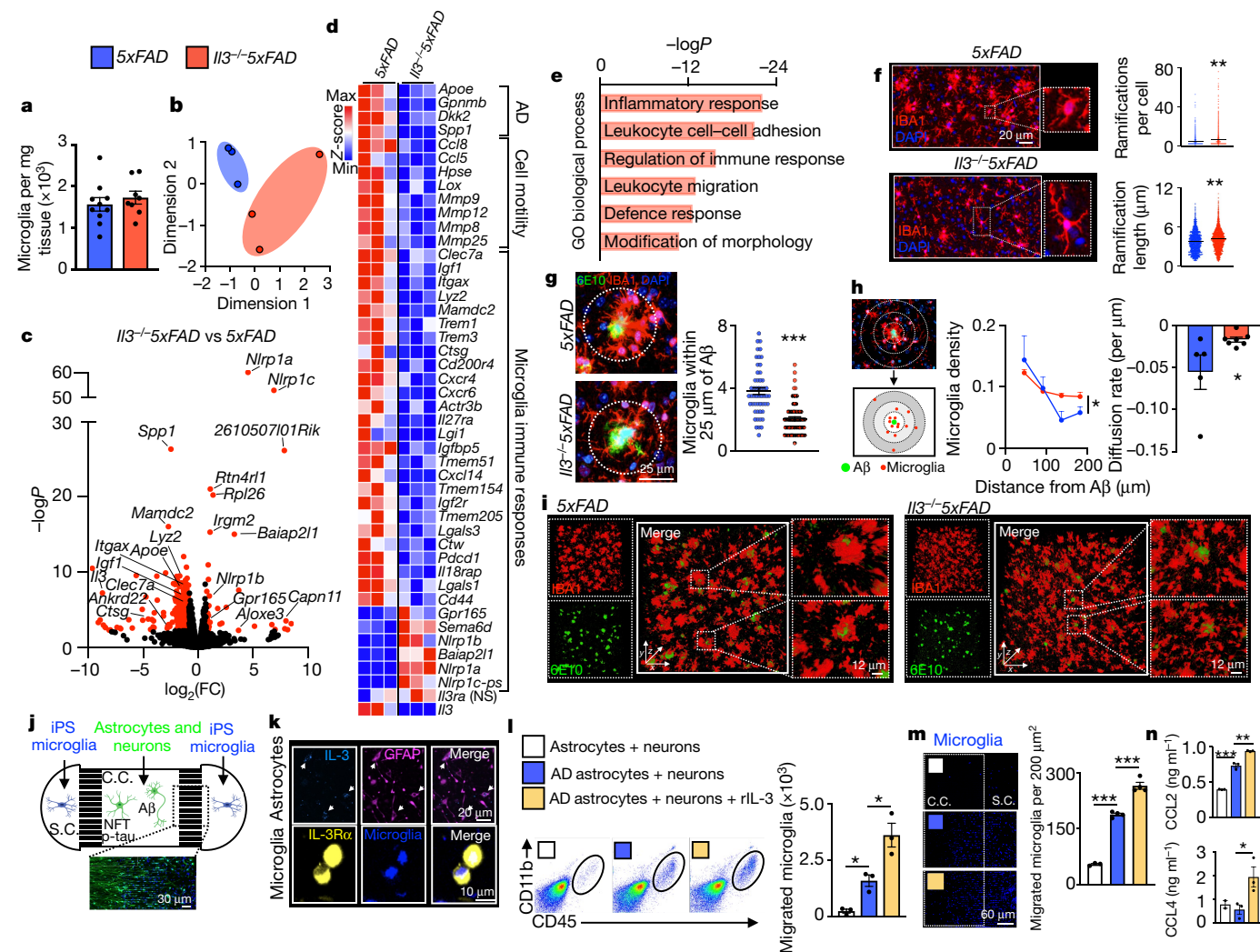
Fig. 4 | IL-3 programs microglia to promote motility and clustering of Aβ in the mouse brain and in a 3D human microfluidic triculture system.
a, Numbers of microglia in *5xFAD* and *Il3⁻/⁻5xFAD* mice (*n* = 10 *5xFAD* mice; *n* = 8 *Il3⁻/⁻5xFAD* mice). **b**, Multidimensional scaling (MDS) plot of RNA-seq data from microglia of 5-month-old *5xFAD* and *Il3⁻/⁻5xFAD* mice (*n* = 12; each data point represents 2M and 2F pooled mice). **c**, Volcano plot of differentially regulated genes (FC > 1.6, FDR < 0.1, *P* < 0.005). **d**, Heat map of key differentially regulated genes, plus *Il3ra* (NS, not significant). **e**, Gene ontology (GO) pathway analysis of differentially regulated genes. **f**, Representative images and skeletal analysis of microglia (*n* = 5 *5xFAD* mice; *n* = 4 *Il3⁻/⁻5xFAD* mice). **g**, Representative images and quantification of microglia within 25 μm of Aβ plaques (*n* = 5 *5xFAD* mice; *n* = 7 *Il3⁻/⁻5xFAD* mice). **h**, Schematic, computed density gradient, and diffusion rate of microglia surrounding Aβ (*n* = 5 *5xFAD* mice; *n* = 7 *Il3⁻/⁻5xFAD* mice). Two-way ANOVA. **i**, Representative 3D images of mouse cortex

(634 × 250 × 634 μm). Groups are of 5-month-old mice of evenly mixed sex. **j**, Scheme of 3D microfluidic system in which human progenitor-derived neurons and astrocytes, with or without AD mutations, are plated in the central chamber (C.C.) while human iPS cell-derived microglia labelled with CellTracker are plated in side chambers (S.C.). **k**, Representative images of IL-3 localization to astrocytes and IL-3Rα to microglia. **l**, Flow cytometry quantification of migrated microglia (in centre chamber) with or without human rIL-3 (*n* = 3). **m**, Representative images and quantification of migrated microglia (*n* = 3 per group for astrocytes + neurons; *n* = 4 AD astrocytes + neurons and AD astrocytes + neurons + rIL-3). **n**, Levels of CCL2 and CCL4 in medium (*n* = 3, except for CCL4 astrocytes + neurons (*n* = 2)). *P* < 0.05, **P* < 0.01, ***P* < 0.001; two-tailed Mann–Whitney *U*-tests unless otherwise indicated; mean ± s.e.m.

Together, these findings suggest that the pathology and severity of AD drive microglia to express *IL3R*A, and indicate that IL-3 signalling is relevant in the human brain during AD pathogenesis.

Having observed dynamic IL-3 signalling in AD, we investigated the protective functions of IL-3. In *5xFAD* mice, *Il3* deletion did not alter the number (Fig. 4a) or the proliferative capacity of microglia (Extended Data Fig. 7a, b). We performed RNA-seq of microglia from *5xFAD* and *Il3⁻/⁻5xFAD* mice and identified 309 genes that were differentially expressed (269 decreased and 40 increased in *Il3⁻/⁻5xFAD* versus *5xFAD*; log₂FC > 1.6, false discovery rate (FDR) < 0.1, *P* < 0.005), and a distinct transcriptional signature of *Il3⁻/⁻5xFAD* microglia (Fig. 4b, c). Microglia from *Il3⁻/⁻5xFAD* mice, despite the increased Aβ burden, had abrogated transcriptional activation of many genes indicative of AD and immune

activation (Fig. 4c, d). Notably, deletion of *Il3* led to reduced expression of *Apoe*, along with repressed expression of genes associated with AD and tissue repair (*Spp1*, *Dkk2*, *Gpnmb*), microglial immune responses (*Clec7a*, *Igf1*, *Itgax*, *Lyz2*, *Mamdc2*, *Actr3b*, *Trem3*, *Trem1*, *Ctsg*, *Ctsw*, *Cd200r4*, *Clec4e*, *Cxcr4*, *Cxcr6*, *IL27ra*), and genes that are essential for cell motility, extracellular matrix remodelling, and dissolution (*Ccl8*, *Ccl5*, *Hpse*, *Lox*, *Mmp9*, *Mmp12*, *Mmp8*, *Mmp25*). IL-3 regulated the immune response, leukocyte migration, and modification of morphology pathways (Fig. 4e). Expression of TREM2-dependent genes (for example, *Spp1*, *Itgax*, *Apoe*, *Lyz2*, *Clec7a*) was altered by *Il3* deletion, but expression of *Trem2* and *Tyrobp* was not (FC = 0.8133, FDR = 0.233 and FC = −0.43, FDR = 0.09, respectively), bolstering the idea that IL-3 signalling acts downstream of TREM2. Collectively, these data show
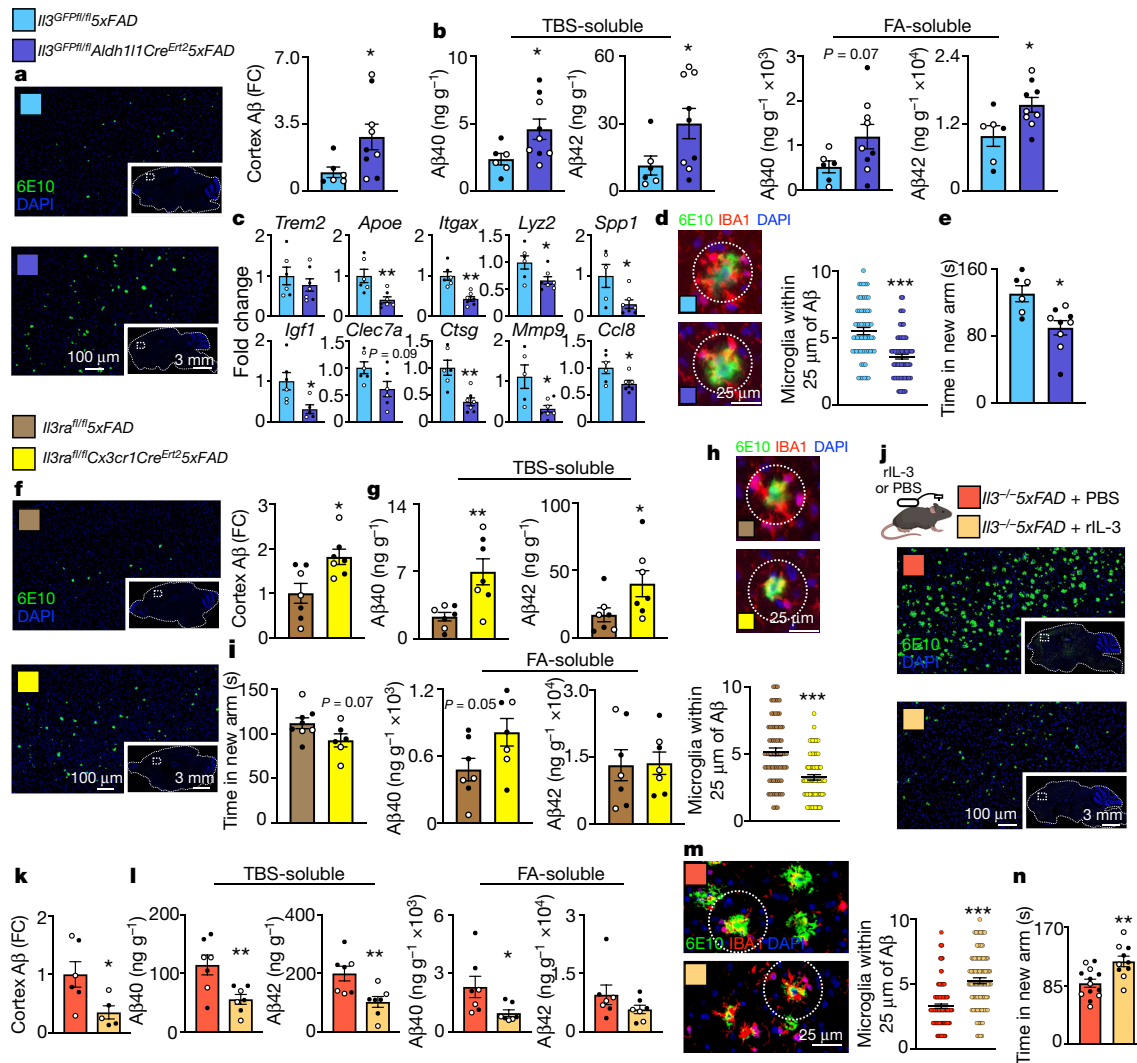
Fig. 5 | Astrocyte IL-3 or microglia IL-3Rα deletion instigate, while IL-3 infusion resolves, Aβ burden and cognitive decline. a, Representative images and Aβ quantification of brain sections from 5-month-old *Il3^GFPfl/fl^5xFAD* (*n* = 6) and *Il3^GFPfl/fl^Aldh1l1Cre^Ert2^5xFAD* mice (*n* = 9) injected with tamoxifen. **b**, Levels of Aβ40 and Aβ42 in cortex homogenates (*n* = 6 *Il3^GFPfl/fl^5xFAD* mice; *n* = 9 *Il3^GFPfl/fl^Aldh1l1Cre^Ert2^5xFAD* mice). **c**, Gene expression in microglia (*n* = 6 *Il3^GFPfl/fl^5xFAD* mice; *n* = 9 *Il3^GFPfl/fl^Aldh1l1Cre^Ert2^5xFAD* mice). **d**, Representative images and quantification of microglia–Aβ co-localization (*n* = 6 *Il3^GFPfl/fl^5xFAD* mice; *n* = 9 *Il3^GFPfl/fl^Aldh1l1Cre^Ert2^5xFAD* mice). **e**, Time in new arm of Y-maze (*n* = 6 *Il3^GFPfl/fl^5xFAD* mice; *n* = 9 *Il3^GFPfl/fl^Aldh1l1Cre^Ert2^5xFAD* mice). **f**, Representative images and Aβ quantification of brain sections from 5-month-old *Il3ra^fl/fl^5xFAD* and *Il3ra^fl/fl^Cx3cr1Cre^Ert2^5xFAD* mice injected with tamoxifen (*n* = 7). **g**, Levels of Aβ40 and Aβ42 in cortex homogenates (*n* = 7). **h**, Representative images and quantification of microglia–Aβ co-localization (*n* = 7). **i**, Time in new arm of Y-maze (*n* = 8 *Il3ra^fl/fl^5xFAD* mice; *n* = 6 *Il3ra^fl/fl^Cx3cr1Cre^Ert2^5xFAD* mice). **j**, Experimental approach and representative images of brain sections probed from mice that received brain infusion of PBS or rIL-3. **k**, Quantification of cortex Aβ (*n* = 6 *Il3^−/−^5xFAD* + PBS; *n* = 5 *Il3^−/−^5xFAD* + rIL-3). **l**, Levels of Aβ40 and Aβ42 in cortex homogenates (*n* = 7). **m**, Representative images and quantification of microglia within 25 μm of Aβ in the cortex (*n* = 6 *Il3^−/−^5xFAD* + PBS; *n* = 5 *Il3^−/−^5xFAD* + rIL-3). **n**, Time in new arm of Y-maze (*n* = 13 *Il3^−/−^5xFAD* + PBS; *n* = 10 *Il3^−/−^5xFAD* + rIL-3). Filled circles, males; open circles, females. *P < 0.05, **P < 0.01, ***P < 0.001; two-tailed Mann–Whitney *U*-tests. Mean ± s.e.m.

that IL-3 induces broad programing of the microglial transcriptome, deploying immune and motile responses.

Given our findings, we tested the role of IL-3 in shaping microglial morphology, motility, and distribution. Microglia in *5xFAD* mice were globular and rounded (Fig. 4f). By contrast, microglia in *Il3^−/−^5xFAD* mice had a ramified morphology with numerous fine elongations, akin to a more homeostatic or resting state. IL-3 deficiency hindered microglial tissue mobilization and suppressed their ability to migrate towards and cluster around Aβ deposits (Fig. 4g). To expand on this observation, we used a watershed algorithm to compute the spatial orientation of microglia relative to Aβ plaques (Fig. 4h). As expected, in *5xFAD* mice we observed high microglial density closest to Aβ, which dissipated precipitously in concentric regions radiating from the plaque. In *Il3^−/−^5xFAD* mice, however, microglial density was more uniform,

resulting in a lower concentration of cells proximal to Aβ and a reduced rate of microglial diffusion. Building on these findings, we performed 3D whole-mount imaging of optically cleared cortical tissue and chose areas with comparable Aβ burden to assess microglial morphology and spatial distribution. In *5xFAD* mice, microglia were globular and clustered Aβ (Fig. 4i, Supplementary Video 1). In *Il3^−/−^5xFAD* mice, microglia were more ramified, disperse, and uniformly distributed, and their ability to cluster Aβ was impaired. The ability of microglia to phagocytose Aβ was independent of IL-3, as we did not observe changes in the expression of genes for machinery that is important for Aβ phagocytosis (for example, *Axl*, *Dcstamp*, *Mertk*, *Cd36*, *Cd47*, *Msra*), or in the ability of microglia to ingest Aβ (Extended Data Fig. 7c, d). In addition, IL-3 did not influence the production of inflammatory cytokines (*Ifng*, *Il18*, *Il1b*, *Il6*, *Tnfα*, Extended Data Fig. 7e). These findings suggest that

Article

IL-3 has a specific role in instigating microglial immune activation, parenchymal redistribution, and clustering around Aβ aggregates, which facilitate the formation of a microglial barrier and Aβ clearance before unresolving tissue-damaging inflammation can be established.

To directly explore the capacity of IL-3 to mediate the motility of human microglia, we used a 3D microfluidic triculture system that mimics the in vivo human AD environment[25,26] (Fig. 4j). The central chamber of the microfluidic system was loaded with human GFP⁺ neurons and astrocytes that had been differentiated from either control progenitor cells or cells engineered to overexpress mutated Aβ precursor protein (AD astrocytes and neurons). In the side chambers, we plated labelled adult microglia derived from human induced pluripotent stem (iPS) cells. The central and side chambers were linked by migration channels. First, we confirmed the presence of mature neurons, astrocytes, and neurofibrillary p-tau tangles along with augmented Aβ in central chambers plated with AD cells (Extended Data Fig. 8a, b). Similar to our observations in mouse and human brains, IL-3 was co-localized with astrocytes and IL-3Rα with iPS microglia (Fig. 4k, Extended Data Fig. 8c). The addition of recombinant (r)IL-3 to the AD tricultures robustly increased the migration of microglia to the central chamber (Fig. 4l, m) and augmented CCL2 and CCL4 levels (Fig. 4n, Extended Data Fig. 8d). Reflecting our in vivo data, these results point to a critical role for IL-3 in the recruitment of microglia to human Aβ aggregates and neurofibrillary p-tau.

Next, we sought to determine the specific contributions of astrocyte IL-3 and microglia IL-3Rα to AD. We generated inducible astrocyte-specific *Il3*-knockout *5xFAD* mice (*Il3^{GFPfl/fl}Aldh1l1Cre^{ERT2}5x-FAD*) and repeatedly injected them with tamoxifen, which blocked astrocyte IL-3 production and reduced CSF IL-3 levels by 75% (Extended Data Fig. 3f–h). Deletion of astrocyte-sourced IL-3 resulted in increased deposition of Aβ (Fig. 5a, b), repressed microglial expression of *Apoe*, *Itgax*, *Lyz2*, *Spp1*, *Igf1*, *Clec7a*, *Ctsg*, *Mmp9*, and *Ccl8* (but not *Trem2*; Fig. 5c), and limited microglial clustering of Aβ (Fig. 5d). Memory was also impaired in these mice (Fig. 5e). To target microglial IL-3Rα, we used a similar CRISPR–Cas9 editing strategy to generate mice with *loxp* sequences flanking *Il3ra* (Supplementary Tables 1–5, Extended Data Fig. 3a–d). We generated inducible microglia-specific *Il3ra*-knockout *5xFAD* mice (*Il3ra^{fl/fl}Cx3cr1Cre^{ERT2}5xFAD*) and repeatedly injected them with tamoxifen to abrogate the appearance of IL-3Rα⁺ microglia (Extended Data Fig. 3i–k). Relative to controls, *Il3ra^{fl/fl}Cx3cr1 Cre^{ERT2}5xFAD* mice had higher Aβ levels (Fig. 5f, g), reduced microglia-Aβ co-localization (Fig. 5h), and a tendency towards worsened memory (Fig. 5i). These findings suggest that IL-3-mediated astrocyte–microglia communication is a key regulator of microglia programing that protects against AD pathology.

Our results raise the possibility of using IL-3 therapeutically. To explore this idea, we stereotactically injected rIL-3 into the cortex of *5xFAD* mice. This led to a robust and rapid (fewer than three days) mobilization of microglia and clustering around Aβ (Extended Data Fig. 9a). We extended this observation by delivering continuous rIL-3 into the lateral ventricle for 28 days, which reduced Aβ load (Fig. 5j–l). Although the number of microglia was unaltered by rIL-3 infusion ($3.4 \pm 0.4 \times 10^3$ versus $2.9 \pm 0.6 \times 10^3$ cells per milligram, PBS versus rIL-3 infusion), clustering of Aβ deposits increased (Fig. 5m) and memory improved (Fig. 5n). The location of delivery was critical, as 10 weeks of peripheral rIL-3 injections did not influence AD pathology (Extended Data Fig. 9b–d). Collectively, these data reveal the therapeutic potential of IL-3 in AD.

The repeated failures of anti-AD therapeutics necessitate the exploration of new pathophysiological mechanisms of disease. Here we describe IL-3 as a mediator of astrocyte–microglia cross-talk, microglia programming, and AD pathology (Extended Data Fig. 9e). These data support the potential targeting of IL-3 signalling to reduce AD-related pathology.

Online content

Any methods, additional references, Nature Research reporting summaries, source data, extended data, supplementary information, acknowledgements, peer review information; details of author contributions and competing interests; and statements of data and code availability are available at https://doi.org/10.1038/s41586-021-03734-6.

1. Linnerbauer, M., Wheeler, M. A. & Quintana, F. J. Astrocyte crosstalk in CNS inflammation. *Neuron* **108**, 608–622 (2020).
2. Vainchtein, I. D. & Molofsky, A. V. Astrocytes and microglia: in sickness and in health. *Trends Neurosci.* **43**, 144–154 (2020).
3. Castellani, G. & Schwartz, M. Immunological features of non-neuronal brain cells: implications for Alzheimer's disease immunotherapy. *Trends Immunol.* **41**, 794–804 (2020).
4. Fakhoury, M. Microglia and astrocytes in Alzheimer's disease: implications for therapy. *Curr. Neuropharmacol.* **16**, 508–518 (2018).
5. Long, J. M. & Holtzman, D. M. Alzheimer disease: an update on pathobiology and treatment strategies. *Cell* **179**, 312–339 (2019).
6. Mindur, J. E. & Swirski, F. K. Growth factors as immunotherapeutic targets in cardiovascular disease. *Arterioscler. Thromb. Vasc. Biol.* **39**, 1275–1287 (2019).
7. Gómez Ravetti, M. & Moscato, P. Identification of a 5-protein biomarker molecular signature for predicting Alzheimer's disease. *PLoS ONE* **3**, e3111 (2008).
8. Ray, S. et al. Classification and prediction of clinical Alzheimer's diagnosis based on plasma signaling proteins. *Nat. Med.* **13**, 1359–1362 (2007).
9. Britschgi, M. et al. Modeling of pathological traits in Alzheimer's disease based on systemic extracellular signaling proteome. *Mol. Cell. Proteomics* **10**, 008862 (2011).
10. Soares, H. D. et al. Plasma biomarkers associated with the apolipoprotein E genotype and Alzheimer disease. *Arch. Neurol.* **69**, 1310–1317 (2012).
11. Huberman, M. et al. Correlation of cytokine secretion by mononuclear cells of Alzheimer patients and their disease stage. *J. Neuroimmunol.* **52**, 147–152 (1994).
12. Kiddle, S. J. et al. Plasma based markers of [11C] PiB-PET brain amyloid burden. *PLoS ONE* **7**, e44260 (2012).
13. Frei, K., Bodmer, S., Schwerdel, C. & Fontana, A. Astrocytes of the brain synthesize interleukin 3-like factors. *J. Immunol.* **135**, 4044–4047 (1985).
14. Frei, K., Bodmer, S., Schwerdel, C. & Fontana, A. Astrocyte-derived interleukin 3 as a growth factor for microglia cells and peritoneal macrophages. *J. Immunol.* **137**, 3521–3527 (1986).
15. Zambrano, A., Otth, C., Maccioni, R. B. & Concha, I. I. IL-3 controls tau modifications and protects cortical neurons from neurodegeneration. *Curr. Alzheimer Res.* **7**, 615–624 (2010).
16. Zambrano, A., Otth, C., Mujica, L., Concha, I. I. & Maccioni, R. B. Interleukin-3 prevents neuronal death induced by amyloid peptide. *BMC Neurosci.* **8**, 82 (2007).
17. Herisson, F. et al. Direct vascular channels connect skull bone marrow and the brain surface enabling myeloid cell migration. *Nat. Neurosci.* **21**, 1209–1217 (2018).
18. Gate, D. et al. Clonally expanded CD8 T cells patrol the cerebrospinal fluid in Alzheimer's disease. *Nature* **577**, 399–404 (2020).
19. Zenaro, E. et al. Neutrophils promote Alzheimer's disease-like pathology and cognitive decline via LFA-1 integrin. *Nat. Med.* **21**, 880–886 (2015).
20. Pasciuto, E. et al. Microglia require CD4 T cells to complete the fetal-to-adult transition. *Cell* **182**, 625–640 (2020).
21. Anzai, A. et al. Self-reactive CD4⁺ IL-3⁺ T cells amplify autoimmune inflammation in myocarditis by inciting monocyte chemotaxis. *J. Exp. Med.* **216**, 369–383 (2019).
22. Zhou, Y. et al. Human and mouse single-nucleus transcriptomics reveal TREM2-dependent and TREM2-independent cellular responses in Alzheimer's disease. *Nat. Med.* **26**, 131–142 (2020).
23. Keren-Shaul, H. et al. A unique microglia type associated with restricting development of Alzheimer's disease. *Cell* **169**, 1276–1290 (2017).
24. Griciuc, A. et al. TREM2 acts downstream of CD33 in modulating microglial pathology in Alzheimer's disease. *Neuron* **103**, 820–835 (2019).
25. Choi, S. H. et al. A three-dimensional human neural cell culture model of Alzheimer's disease. *Nature* **515**, 274–278 (2014).
26. Park, J. et al. A 3D human triculture system modeling neurodegeneration and neuroinflammation in Alzheimer's disease. *Nat. Neurosci.* **21**, 941–951 (2018).

Methods

No statistical methods were used to predetermine sample size. Experiments were randomized whenever possible and investigators were blinded to allocation during experiments and outcome assessment whenever possible.

Human samples

Frozen tissue specimens and paraffin sections from the frontal cortex of patients with AD and age-matched control donors without dementia were obtained from the Massachusetts Alzheimers Disease Research Center Brain Bank. Subjects or next of kin consented to the brain donation and the Massachusetts General Hospital Institutional Review Board approved the study. All patients with AD met the National Institute of Neurological and Communicative Disorders and Stroke–Alzheimer's Disease and Related Disorders Associations criteria for probable AD and the National Institute on Ageing–Reagan Institute criteria for high likelihood of AD. Secondary use of de-identified human samples was approved by the institutional review board of the Massachusetts General Hospital (protocol nos. 2019P003736 and 2019P003732).

Mice

Wild-type C57BL/6J, B6;FVB-Tg(Aldh1l1-EGFP/Rpl10a)JD130Htz/J, C57BL/6J-Trem2em2Adiuj/J, B6.129P2(C)-Cx3cr1tm2.1(cre/ERT2)Jung/J, B6N.FVB-Tg(Aldh1l1-cre/ERT2)1Khakh/J and C57BL/6-Tg(UBC-GFP)30Scha/J mice were purchased from The Jackson Laboratory. *5xFAD* mice[27] were purchased from the Jackson Laboratory (MMRRC) and backcrossed onto the C57BL/6J background for more than 10 generations before being crossed with other strains. *Il3*^{-/-} mice on the C57BL/6J background were bred in-house[21,28] and crossed with *5xFAD* mice. For RNA-seq studies, *Trem2*^{-/-} mice[29] on the C57BL/6J background were generated at Washington University School of Medicine, bred in-house, and crossed with *5xFAD* mice. Age- and sex-matched mice were used. If the sex of the animals is not specifically indicated, groups were sex-balanced. Where appropriate, mice were randomly assigned to interventions. All mice were group-housed under standard conditions with free access to food and water. All animal protocols were approved by the Animal Review Committee at the Massachusetts General Hospital (protocol nos. 2011N000035 and 2015N000044) and were in compliance with relevant ethical regulations.

CRISPR–Cas9 generation of *Il3*[GFPfl/fl] and *Il3ra*^{fl/fl} mice.

Two SpCas9 guide RNAs (gRNAs; Supplementary Table 1) were initially designed to target genomic regions within the first intron and 3′ of the stop codon of *Il3* and *Il3Rα* genes, using on-target and off-target prediction software[30,31]. Single-stranded DNA (ssDNA) donor oligos encoding the floxed cDNA were designed for *Il3* and *Il3rα* (Extended Data Fig. 3a, b), both of which encoded a P2A-*eGfp* tag and ~500 base pair homology arms on either end (synthesized by Genewiz; Supplementary Information 1 and 2). Prior to performing experiments with the ssDNA donors, the on-target activities of the gRNAs were evaluated by microinjection of ribonucleoprotein (RNP) complexes comprised of TrueCut Cas9 v2 (ThermoFisher) and synthetic gRNAs (Synthego) into mouse zygotes. All microinjections were performed at the Genome Modification Facility (Harvard University). Injected zygotes developed to the blastocyst stage before genomic DNA extraction. To evaluate genome editing efficiencies, the target regions were amplified by PCR using the primers listed in Supplementary Table 2. Amplicons were sent for Sanger sequencing and the approximate level of on-target activity was determined using inference of CRISPR edits (ICE)[32]. The most effective gRNA of each pair examined (within the first intron and 3′ of the stop codon of either *Il3* and *Il3Rα* genes) was then used for microinjections in the presence of the ssDNA donors. Injected embryos were implanted into pseudopregnant recipients, and 17 and 24 pups for the *Il3* and *Il3Rα* targeted mice, respectively, were genotyped at

3 weeks of age. To genotype mice, genomic DNA was extracted from tail snips in 200 µl tail lysis buffer (100 mM Tris-HCl, 200 mM NaCl, 5 mM EDTA, 0.05% SDS, 12.5 mM DTT, 1.4 µg/µl Proteinase K (New England Biolabs)) via ~16 h incubation at 55 °C. Lysates were cleaned up using 0.7× paramagnetic beads prepared as previously described[33,34]. Insertions of the donor DNA sequences into the endogenous *Il3* and *Il3Rα* loci (Extended Data Fig. 3a, b) were confirmed by Sanger sequencing across the full donor sequence (using the primers in Supplementary Table 3). Founder mice in which the full-length insert was detected were then selected for further breeding to remove mosaicism and generate *Il3*[GFPfl/fl] and *Il3rα*^{fl/fl} N1 mice. Sanger sequencing revealed missense mutations in the inserted sequence that were not present in the ssDNA donor sequence (Supplementary Table 4). Missense mutations resulted in the quenching of the GFP signalling in *Il3rα* targeted mice but did not influence IL-3Rα functionality or signalling (Extended Data Fig. 3i). GFP functionality remained intact in *Il3*-targeted mice (Fig. 2b, f, Extended Data Fig. 3e) Subsequent *Il3*[GFPfl/fl] and *Il3rα*^{fl/fl} mice were genotyped by PCR via the genotyping strategy and primers in Supplementary Table 5. *Il3*[GFPfl/fl] mice were crossed to *Aldh1l1Cre*[ERT2] and *5xFAD* mice to generate *Il3*[GFPfl/fl]*Aldh1l1Cre*[ERT2]*5xFAD* mice, and *Il3rα*^{fl/fl} mice were crossed to *Cx3cr1Cre*[ERT2] and *5xFAD* mice to generate *Il3rα*^{fl/fl} *CX3Cr1Cre*[ERT2]*5xFAD* mice.

In vivo interventions

Parabiosis. The procedure was conducted as previously described[35]. In brief, age-, sex-, and weight-matched animals were used and housed together for at least 14 days before surgery. The corresponding lateral aspects of each mouse were shaved, incisions were made from the forelimb joint to the hindlimb joint and the subcutaneous fascia was bluntly dissected to create 0.5 cm of free skin. Fore- and hindlimb joints were joined and the dorsal and ventricle skins were approximated by continuous suture using mononylon 5.0 (Ethicon).

LPS injection. Mice were injected daily intraperitoneally with 20 µg lipopolysaccharide (LPS, Sigma) for 4 days.

BrdU injection. Mice were injected intraperitoneally with 1.5 mg bromodeoxyuridine (BrdU, Sigma) twice a day for 5 days.

Recombinant IL-3 brain infusion. A cannula and osmotic minipump (Alzet) were implanted as previously described[36]. In brief, mice were anaesthetized and the head was shaved and secured in a stereotactic frame (Stoelting). An incision was made above the skull extending behind the shoulder blades. A small hole was drilled into the skull at AP −1; ML −0.27 from bregma and depth 2 mm from dura to target the lateral ventricle. The cannula was inserted and glued to the skull. The cannula was connected to an osmotic minipump filled with rIL-3 (Biolegend) conjugated to an anti-IL-3 antibody (Biolegend) as previously described[28]. Minipumps delivered rIL-3 into the ventricle at a rate of 1 µg/day. Minipumps were implanted subcutaneously caudal to the shoulder blades. At the end of the procedure the incision was sutured using mononylon 5.0 (Ethicon).

Stereotactic injection. Mice were anaesthetized and the head was shaved and secured in a stereotactic frame (Stoelting). An incision was made above the skull and a hole was drilled at AD −0.1; ML −0.1 from bregma and depth 0.1 mm from dura to target the cortex. Using a 0.5-µl Hamilton syringe, 3 µg of interleukin-3 (Biolegend) conjugated to an anti-interleukin-3 antibody (Biolegend) was delivered in a volume of 0.5 µl. Regions of the cortex a minimum 600 µm from the injection site were analysed.

Peripheral rIL-3 injection. Mice were injected intraperitoneally with 10 µg rIL-3 (Biolegend) conjugated to an anti-IL-3 antibody (Biolegend) twice a week for 10 weeks.

Article

Cerebrospinal fluid collection. Mice were anaesthetized and the skin of the neck was shaved and disinfected with 70% ethanol. Mice were placed in a stereotactic frame (Stoelting) to secure their heads. A skin incision was made at the back of the neck and muscle layers were retracted to expose the cisterna magna. Cerebrospinal fluid was collected by piercing the pia mater with a microcapillary tube (VWR) and allowing CSF to collect in the capillary.

FITC-dextran injection. Mice were injected intravenously with FITC-dextran (molecular weight 4,000, Sigma Aldrich). Four hours later, mice were perfused with 20 ml PBS at a rate of 5 ml/min. Brain tissue was removed and homogenized and the FITC signal was measured by spectrophotometry in tissue supernatant.

PE–anti-GR1 injection. Mice were injected intravenously with an anti-GR1 antibody conjugated to PE (Biolegend). Four hours later, mice were perfused with 10 ml PBS and the leukocyte fraction was isolated from brain tissue before flow cytometry analysis.

Tamoxifen injection. Tamoxifen (20 mg/ml, Sigma Aldrich) was prepared in corn oil and allowed to dissolve at 37 °C overnight while shaking. Mice were injected i.p. with 2 mg tamoxifen on four consecutive days at 2 months of age, and then monthly thereafter until death at 5 months of age.

Cells

Mouse cell collection. Peripheral blood was collected by retro-orbital bleeding and red blood cells were lysed in RBC lysis buffer (Biolegend). Bone marrow cells were collected by flushing bones with PBS, after which a single-cell suspension was created by passing cells through a 26-gauge needle and red blood cells were lysed with RBC lysis buffer. The brain was excised after perfusion with PBS (Thermo Fisher Scientific), minced and digested with 450 U ml^{-1} collagenase I, 125 U ml^{-1} collagenase XI, 60 U ml^{-1} DNase I and 60 U ml^{-1} hyaluronidase (Sigma) in PBS for 40 min at 37 °C. Samples were passed through a 70-μm cell strainer and mixed with 30% percol layered on top of 70% percol. The percol gradient was centrifuged at 500g for 30 min with the brake off. The cell fraction was collected and washed with PBS before downstream applications. Total viable cell numbers were counted using trypan blue (Cellgro, Mediatech) or counting beads (Thermo Fisher Scientific).

Mouse flow cytometry. Single-cell suspensions were stained in PBS supplemented with 2% FBS and 0.5% BSA. The following monoclonal antibodies were used for flow cytometry analyses at a dilution of 1/700 unless otherwise indicated: anti-CD45 (BioLegend, clon e30-F11, 103147), anti-CD3 (BioLegend, clone 17A2, 100206), anti-CD90.2 (BioLegend, clone 53-2.1, 105308), anti-CD19 (BioLegend, clone 6D5, 115508), anti-B220 (BD Biosciences, clone RA3-6B2, 553089), anti-NK1.1 (BioLegend, clone PK136, 108708), anti-Ly-6G (BioLegend, clone 1A8, 127614), anti-Ly-6C (BioLegend, AL-21, 128006), anti-MHCII (BioLegend, clone M5/114.152, 107602), anti-CD11b (BioLegend, clone M1/70, 101226), anti-CD115 (BioLegend, clone AFS98, 135517), anti-TER119 (BioLegend, clone TER-119, 116208), anti-CD34 (eBioscience, clone RAM34, 11-0341-85), anti-CD49B (BioLegend, clone DX5, 1089008), anti-CD11C (BioLegend, clone N418, 117310), anti-IL-7Rα (BioLegend, clone SB/199, 121112), anti-CD16/32 (BioLegend, clone 93, 101324), anti-CD150 (BioLegend, clone TC15-12F12.2, 115922), anti-cKIT (BioLegend, clone 2B8, 105814), anti-CD135 (BioLegend, clone A2F10, 135310), anti-CD48 (BioLegend, clone HM48-1, 103426), anti-SCA1 (BioLegend, clone D7, 108126), anti-IL-3 (1/100, BD Bioscience, clone MP2-8F8, 55483), anti-IL-3Rα (1/100, eBioscience, clone 6H6, 14-1239-82), anti-GFAP (eBioscience, G5A, 53-982-80), anti-CCL2 (eBioscience, clone 2H5, 11-7096-81), anti-Aβ (BioLegend, clone 6E10, 803013), anti-TREM2 (R&D Systems, clone 237920, FAB17291P), anti-CD11C (BioLegend, clone N418, 117333),

anti-BrdU (eBioscience, clone BU20A, 17-5071-42). BrdU staining and intracellular staining were performed using a commercial kits according to the manufacturer's instructions (BD Bioscience). Viable cells were identified as unstained with Zombie Aqua (BioLegend) or 7AAD (BioLegend). Data were acquired on a LSRII (BD Biosciences) and analysed with FlowJo (Tree Star).

Mouse flow cytometry gating. Live, singlet $c$ells were identified as (1) Ly-6C^{high} monocytes (CD45$^+$CD11b$^+$CD115$^+$Ly-6C^{high}), (2) neutrophils (CD45$^+$CD11b$^+$Ly-6G$^+$), (3) B cells (CD45$^+$B220$^+$CD19$^+$CD11b$^-$), (4) T cells (CD45$^+$CD3$^+$CD90$^+$CD11b$^-$), (5) LSK cells (CD45$^+$Lin$^-$Kit$^+$SCA1$^+$), (6) multipotent progenitor (MPP)4 (CD45$^+$Lin$^-$Kit$^+$SCA1$^+$CD135$^+$CD150$^-$), (7) MPP3 (CD45$^+$Lin$^-$Kit$^+$SCA1$^+$CD135$^+$CD150$^-$CD48$^+$), (8) short-term haematopoietic stem cells (CD45$^+$Lin$^-$Kit$^+$SCA1$^+$CD135$^-$CD150$^-$CD48$^-$), (9) long-term haematopoietic stem cells (CD45$^+$Lin$^-$Kit$^+$SCA1$^+$CD135$^+$CD150$^+$CD48$^-$), (10) common myeloid progenitor (CD45$^+$Lin$^-$Kit$^+$SCA1$^-$CD34$^+$CD16/32^{mid}), (11) granulocyte–macrophage progenitor (CD45$^+$Lin$^-$Kit$^+$SCA1$^-$CD34$^+$CD16/32^{high}CD115$^-$), (12) monocyte–dendritic cell progenitor (CD45$^+$Lin$^-$Kit$^+$SCA1$^-$CD34$^+$CD16/32^{high}CD115$^+$), (13) microglia (CD45^{mid}CD11b$^+$), (14) astrocytes (CD45$^-$CD11b$^-$GFAP$^+$ or CD45$^-$CD11b$^-$ALDH1L1–GFP$^+$), (15) other brain cells (CD45$^-$CD11b$^-$GFAP$^-$ or CD45$^-$CD11b$^-$ALDH1L1–GFP$^-$). Lin is B220, CD19, CD49B, TER119, CD90.2, CD11b, CD11C Ly6G, IL-1Rα.

Cell sorting. Brain cell suspensions were stained to identify the indicated cell populations and cells were sorted on a FACS Aria II cell sorter (BD Biosciences) directly into collection medium.

Ex vivo cell cultures. Sorted microglia were cultured in complete medium (RPMI-1640 supplemented with 10% FBS, 2 mM L-glutamine, 10 U ml^{-1} penicillin and streptomycin, 10 mM HEPES, 50 μM 2-mercaptoethanol, 1 mM sodium pyruvate and 1× nonessential amino acids) and kept in a humidified 5% CO$_2$ incubator at 37 °C. Microglia were exposed to 20 ng/ml rIL-3 (Biolegend) and/or 2 μg/ml Aβ (1–42) HiLyte conjugated to pHrodo iFL red (Invitrogen) for 3 h.

Naive T cells were isolated from the spleen and lymph nodes using a Naive T cell isolation kit (Miltenyi Biotec), cultured on anti-CD3 (2 μg/ml)-coated plates in the presence of soluble anti-CD28 (2 μg/ml) and rmIL-2 (10 μg/ml) for 3 days and re-stimulated with PMA (100 ng/ml) and ionomycin (500 ng/ml) in the presence of GolgiPlug and GolgiStop (1:1,000) for 3.5 h before cell surface staining and analysis.

RNA-seq of WT, *Trem2$^{-/-}$*, *5xFAD*, and *Trem2$^{-/-}$5xFAD* mice

Microglia isolation and fluorescence-activated cell sorting. Microglia were isolated from 4- and 8-month-old WT, *Trem2$^{-/-}$*, *5xFAD* and *5xFADTrem2$^{-/-}$* mice as previously described[24]. In brief, mice were deeply anaesthetized with CO$_2$ and transcardially perfused with PBS/ 1 mM EDTA. Brains were placed into a GentleMacs C-tube (Miltenyi Biotech) with pre-warmed RPMI 1640 medium (Gibco) containing Dispase (2 U/ml), and collagenase type 3 (200 U/ml, Worthington Biochemical Corporation). Using the GentleMACS Dissociator (Miltenyi Biotech), brains were subjected to three rounds of dissociation, each followed by a period of incubation at 37 °C. After the second round of dissociation, DNase I grade II (Roche) was added to a final concentration of 40 U/ml and incubated at 37 °C. After the third round of dissociation, the enzymes were inactivated by adding PBS containing 2 mM EDTA and 5% fetal bovine serum. The brain tissue was triturated, passed through a 100-μm filter (Thermo Fisher Scientific) and centrifuged. Cell pellets were resuspended in 10.5 ml RPMI 1640 medium (Gibco), mixed gently with 4.5 ml physiologic Percoll (Sigma), and centrifuged at 850g for 40 min. Subsequently, cells were rinsed with PBS/1 mM EDTA and centrifuged at 500g for 8 min. Contaminating red blood cells were lysed with red blood cell lysing buffer (Sigma). Cells were rinsed with PBS/1 mM EDTA and centrifuged at 500g for 8 min. Cell pellets were resuspended in blocking buffer (PBS/1 mM EDTA/2% donkey serum) containing Fc

block (1 μg/ml, anti-mouse CD16/32, clone 93, Biolegend) and incubated in ice for 10 min. Then, cells were labelled with Alexa647–anti-CD11b (5 μg/ml, clone M1/170, Biolegend) and Alexa488–anti-CD45 (5 μg/ml, clone 30-F11, Biolegend) antibodies for 30 min on ice. Cells were rinsed and centrifuged at 400g for 8 min. Cells were resuspended in PBS/ 1.0 mM EDTA and sorted by CD11b/CD45 expression using FACS ARIA (BD Biosciences). Cells sorted by fluorescence-activated cell sorting (FACS) were centrifuged at 600g for 10 min and cell pellets were used for RNA extraction.

RNA purification. RNA purification from microglial samples and mRNA sequencing were performed as previously described[24]. In brief, microglial cell pellets were lysed in RLT-Plus buffer (Qiagen) containing 1% β-mercaptoethanol. Cell lysates were transferred to QIAshredder (Qiagen) for homogenization and centrifuged at 18,000g for 2 min. RNA was isolated using the RNeasy Plus Micro Kit (Qiagen). During the RNA extraction protocol, samples were treated with RNase-free DNase I (Qiagen) directly on the RNeasy spin columns at room temperature for 15 min and washed with buffer RW1 (Qiagen). Each RNA sample was eluted in RNase-free water (15 μl, Qiagen) and RNA integrity was assessed with the Agilent RNA 6000 Pico Chip on the 2100 Bioanalyzer (Agilent). Purified RNA was quantified using the Qubit RNA High Sensitivity Assay Kit (Invitrogen) on the Qubit Fluorometer 3.0 (Thermo Fisher Scientific). Microglial RNA samples originating from mice of the same genotype, sex and age were pooled as needed to generate samples containing 100 ng RNA. cDNA libraries were prepared using the TruSeq Stranded mRNA LT Prep Kit (Illumina). The protocol consisted of mRNA purification with poly-T-oligo-attached magnetic beads, mRNA fragmentation, first and second strand cDNA synthesis, 3′ end adenylation, adaptor ligation, and PCR amplification (11 cycles). Libraries were enriched using the Agencourt AMPure XP beads (Beckman Coulter). cDNA libraries were validated using the Agilent DNA 1000 kit on the 2100 Bioanalyzer (Agilent) and quantified by qPCR before sequencing. Libraries were sequenced on a HiSeq 2500 instrument (Illumina) at the MGH Next Generation Sequencing Core Facility, using single-end 50-bp sequencing.

RNA-seq analysis. RNA sequencing resulted in 48.7 million reads per sample on average as previously described[24]. The raw reads of the sequencing data were submitted to NCBI-GEO under accession number GSE132508. The splice-aware alignment program STAR was used to map sequencing reads (fastqs) to the mouse (mm10) reference genome. Gene expression counts were calculated using the program HTSeq based on the latest Ensembl annotation for mm10/GRCm38. The R package edgeR was used to make differential gene expression calls from these counts at a twofold cut-off and FDR < 0.05 threshold. Gene expression was considered upregulated if $log_2FC > 1$ or downregulated if $log_2FC < -1$ (FC denotes fold-change of reads per kilobase per million (RPKM)) at FDR < 0.05. To extract expression data for genes of interest, we used the Python Data Analysis Library (Pandas), a powerful tool for indexing and parsing large data frames.

RNA-seq of *5xFAD* and *Il3⁻/⁻5xFAD* mice
Microglia were sorted by FACS from brains of 5-month-old mice as described above. Microglia were isolated from 12 *5xFAD* mice (6M/6F) and 12 *Il3⁻/⁻5xFAD* mice (6M/6F). Within each genotype, samples from 2M and 2F were pooled to generate three samples each from *5xFAD* and *Il3⁻/⁻5xFAD* mice, from which RNA was isolated and RNA-seq performed. RNA was isolated using E.Z.N.A. micro elute total RNA kit according to the manufacturer's instructions (Omega Biotek). cDNA libraries were prepared using the TruSeq Stranded mRNA LT Prep Kit (Illumina). Libraries were sequenced on a HiSeq 2500 instrument (Illumina) at the MGH Next Generation Sequencing Core Facility, using paired-end 50-bp sequencing. Sequencing reads were mapped in a splice-aware fashion to the Ensembl annotation of the mouse GRCm37/mm9 transcriptome.

Read counts over transcripts were calculated using HTseq followed by differential expression analysis using EdgeR. Genes were classified as differentially expressed based on the cutoffs of FC > 1.6, FDR < 0.1, and P < 0.005.

Gene enrichment analysis. Gene enrichment analysis was done using Enrichr (https://maayanlab.cloud/Enrichr/) with default parameters.

Human iPS triculture microfluidic system
Microfluidic device fabrication. Negative photoresists SU-8 10 and SU-8 100 (MicroChem, Newton, MA, USA) were sequentially patterned using standard lithography on a 4-inch (10.16-cm) silicon wafer to create a mould for cell migration channels of 10 μm height and central/ side chambers of 100 μm height. The base and a curing agent were mixed at a 10:1 weight ratio (SYLGARD 184 A/B, Dow corning), poured onto the SU-8 mould, and cured for 1 h at 25 °C under vacuum and, subsequently, cured for more than 3 h in an oven at 80 °C. The cured poly dimethyl-siloxane (PDMS) replica was peeled off the mould and 4-mm holes were punched for cell-containing chambers. PDMS and glass slides were assembled, irreversibly, using oxygen plasma at 50 mW, 5 cm, for 30 s (PX-250, March Plasma Systems). Immediately after the bonding, 50 μl of diluted BD Matrigel (1:100, BD Biosciences) in DMEM/F12 was injected into each hole and incubated for 2 h at 25 °C to promote cellular adhesion. The PLL-treated surface was rinsed with autoclaved and 0.2-μm-filtered water (AM9920, Life Technologies).

3D cell cultures and differentiation of neural progenitor cells. ReN cell VM human neural progenitor cells (NPCs) with or without the K670N/M671L (Swedish) and V717I (London) familial AD mutations were purchased from EMD Millipore (SCC008). The source of cell lines were validated by Millipore-Sigma. Unbiased RNA-seq analysis was performed for cell lines to confirm the expression of AD mutations. All cell lines were regularly tested for mycoplasma and were negative. AD mutations result in overproduction of Aβ and neurofibrillary tangle (NFT) p-tau. For 3D cultures, BD Matrigel (BD Biosciences) was mixed with the cells (1×10^6 cells per ml). The final cell concentration for the mixture was approximately 5×10^4 cells per ml (1:5 3D thin-culture). We then transferred 10 μl of cell mixture into the microfluidic device using prechilled pipettes. The microfluidic devices were incubated for 1 h at 37 °C during gel solidification and then 100 μl differentiation medium was added[25,26]. Differentiation medium was composed of DMEM/ F12 (Life Technologies) supplemented with 2 mg heparin (StemCell Technologies), 2% (v/v) B27 neural supplement (Life Technologies), 20 mg EGF (Sigma), 20 mg bFGF (Stemgent), and 1% (v/v) penicillin/ streptomycin/amphotericin-B solution (Lonza). The 3D-plated cells were differentiated for 4 weeks; medium was changed every 3–4 days.

Microglia preparation. To generate induced microglia-like cells (iM-GLs), we used iPS cells (BIOQ Subject ID: NDS00159) obtained from NINDS iPSC cell repository (distributed through RUCDR, https:// www.rucdr.org). In brief, improved and simplified differentiation of iPSCs to CD43⁺ primitive haematopoietic progenitor cells (HPCs) was achieved using Stem Cell Technologies STEMdiff Haematopoietic Kit (catalog no. 05310)[37]. On day −1, feeder-free iPSCs that had been expanded in TeSR-E8 medium were passaged with ReLeaSR (STEMCELL Technologies) into mTeSR E8 medium with 0.5 μM Thiazovivin onto matrigel-coated (1 mg/ml) 6-well plates (Corning Costar). Small aggregates of ~100 cells each were plated at 10–20 aggregates per cm². Medium B (1 ml) was supplemented until day 24. On day 25, cells were centrifuged, leaving 1 ml conditioned medium per 35-mm well. On day 25, cells were re-suspended in microglia medium plus 100 ng/ml IL-34, 50 ng/ml TGFβ1, 25 ng/ml M-CSF, 100 ng/ml CD200 and 100 ng/ml CX3CL1 to further mature microglia and ensure homeostasis. On day 27, microglia medium with the five cytokine cocktails was added (1 ml per well). iPS-derived microglia were validated with the expression

of microglia markers P2RY12, TREM2, and IBA1 independently. All cell lines were regularly tested for mycoplasma and were negative. Before the experiment, cells were incubated with CellTracker Deep Red Dye (10 µM in DMSO, C34565, Invitrogen) for 30 min and washed using medium without serum. After centrifugation (200g for 5 min), the cells were resuspended in 1 ml microglia medium (1×10^6 cells/ml). We injected 10 µl of the cell suspension into each side chamber and 100 µl of a culturing medium was added to the side chambers. The loaded 3D microdevices were then incubated at 37 °C with 5% CO_2.

Recombinant IL-3 treatment. For treatment with human rIL-3 (Abcam), NPC differentiation medium containing 15 µg IL-3 was added to 3-week differentiated 3D culture in the central chamber. Recombinant IL-3 was maintained in the medium for an additional 2 weeks throughout the migration experiment.

Time-lapse imaging. After microglia loading, cells were recorded using time-lapse imaging using a fully automated Nikon C2s confocal laser scanning microscope (Nikon Instruments Inc.) with an incubator heated to 37 °C and 5% CO_2 (20× magnification; Micro Device Instruments, Avon, MA, USA).

Flow cytometry. Cells from the central chamber were collected and repeatedly pipetted in medium to break up Matrigel. Cells were centrifuged and washed with PBS. The single-cell suspensions were stained with antibodies in PBS. The following monoclonal antibodies were used at a dilution of 1:700 for flow cytometry analyses: anti-mouse/human CD45 (BioLegend, clone30-F11, 103147), anti-mouse/human CD11b (BioLegend, clone M1/70, 101226). CountBright absolute counting beads (Invitrogen) were added to the cell suspension to enumerate cells. Microglia were identified as live CD11b⁺CD45⁺ cells. Data were acquired on a LSRII (BD Biosciences) and analysed with FlowJo (Tree Star).

MSD ELISA Aβ and chemokine measurement. Levels of Aβ38, Aβ40 and Aβ42 in medium were simultaneously measured by a multi-array electrochemiluminescence assay kit (K15200E-2, V-PLEX Aβ Peptide Panel 1 (6E10) kit, Meso Scale Diagnostics (MSD)). To quantify Aβ levels in differentiation medium, conditioned medium from the central chamber was collected for each condition, diluted 1:6 with MSD dilution buffer, and analysed using the assay kit. A Human Chemokine Array (K15047G-1, MSD) kit was used to simultaneously detect the relative expression of 10 human chemokines. Conditioned medium (20 µl from each sample) was collected and analysed according to the manufacturer's protocol.

Immunostaining. For immunofluorescent stains, we rinsed the cells and 3D cultures twice with PBS (phosphate-buffered saline). Cells were then fixed at room temperature (30 min incubation in fresh 4% paraformaldehyde aqueous solution (157-4, Electron Microscopy Sciences) followed by rinsing twice with PBS). Cells were permeabilized through incubation in 0.1% Triton X-100 in PBST (phosphate-buffered saline with 0.1% Tween 20) for 15 min at room temperature. Cell-specific binding was blocked through overnight incubation in 3% human serum albumin in PBST at 4 °C. After 24-h incubation with the primary antibody solutions at 4 °C, the cells were washed five times. The following antibodies (and dilutions) were used: anti-PHF (1:1,000, a gift from P. Davies, Albert Einstein College of Medicine), anti-GFAP (1:500, Millipore), anti-P2RY12 (1:400, Sigma), anti-IL-3Rα (1:200, Biolegend), anti-β-tubulin III (1:200, Abcam) and anti-IL-3 (1:200, Invitrogen).

Histology
Mouse. Brains were removed and fixed in 10% formalin overnight. The fixed brains were paraffin-embedded and sectioned in the sagittal plane. The paraffin-embedded sections were deparaffinized and rehydrated before immunofluorescent staining. Heat-induced antigen retrieval was performed using Retrievagen A (pH6.0) (550524, BD Biosciences), and the sections were permeabilized with 0.3% Triton X-100 in PBS for 10 min at room temperature. After the sections were blocked with 4% normal goat serum in PBS, primary antibodies, IBA1 (1:200, 019-19741, FUJIFILM Wako Chemicals) and Alexa Fluor 488 anti-β-amyloid, 1–16 (1:250, 803013, 6E10, BioLegend), were incubated at 4 °C overnight. A biotinylated goat anti-rabbit IgG secondary antibody and streptavidin DyLight 594 (1:100, BA-1000 and 1:600, SA-5594, Vector Laboratories) were applied to detect IBA1. Brains from *Aldh1l1^GFP^*, *Il3^GFPfl/fl^*, *Il3^−/−^* and WT mice were removed and fixed in 4% paraformaldehyde solution at 4 °C overnight. After rinsing with PBS, the fixed brains were placed in 30% sucrose in PBS at 4 °C overnight. The brains were embedded in OCT compound and serial frozen sections (10 µm) were prepared using CryoJane Tape Transfer System (Leica Biosystems). For *Aldh1l1^GFP^* and *Il3^GFPfl/fl^* mice, an anti-GFP antibody (1:400, ab13970, Abcam) and a goat anti-chicken IgY secondary antibody, Alexa Fluor 488 (1:100, A-11039, Thermo Fisher Scientific) were used to detect GFP–ALDH1L1 and GFP–IL-3. An anti-IL-3 antibody (1:5, 503902, MP2-8F8, BioLegend) followed by a biotinylated rabbit anti-rat IgG secondary antibody and streptavidin DyLight 594 (1:100, BA-4001 and 1:600, SA-5594, Vector Laboratories) were used for IL-3 detection in *Aldh1l1^GFP^* mice. A GFAP, eFluor 615 monoclonal antibody (1:25, 42-9892-80, GA5, Thermo Fisher Scientific) was used to detect astrocytes from *Il3^GFP^* mice. For co-localization of IL-3Rα with IBA1, an anti-IL-3Rα antibody (1:50, 141039, US Biological) and an anti-IBA1 antibody (1:50, ab5076, Abcam) were incubated at 4 °C overnight after blocking with 4% donkey serum in PBS. A donkey anti-rabbit IgG secondary antibody, Alexa Fluor 555 (1:100, A-31572, Thermo Fisher Scientific) and a donkey anti-goat IgG secondary antibody, Alexa Fluor 488 (1:100, A-11055, Thermo Fisher Scientific) were used to detect IL-3Rα and IBA1, respectively. An Alexa Fluor 647 anti-β-amyloid, 1–16 antibody (1:50, 803021, 6E10, BioLegend) was used to identify amyloid plaques in the brains. For *Il3^−/−^* and WT mice, doublecortin (1:400, 4604S, Cell Signaling Technology) and active caspase-3 (1:50, 559565, C92-605, BD Biosciences) were stained to detect neuronal precursor cells and apoptotic cells, respectively. A biotinylated goat anti-rabbit IgG secondary antibody and streptavidin DyLight 594 (1:100, BA-1000 and 1:600, SA-5594, Vector Laboratories) were used for the staining. Nuclei were counterstained with DAPI (1:3,000, D21490, Thermo Fisher Scientific). The images were captured using a digital scanner Nano-Zoomer 2.0RS (Hamamatsu, Japan) or an automated fluorescence microscope, BX63 (Olympus). Image analysis and quantification were done with ImageJ software. Microglia morphology analysis was done using the Skeletonize plug-in for ImageJ.

Mouse whole-mount 3D confocal imaging. Brains were removed from 5-month-old *5xFAD* and *Il3^−/−^5xFAD* mice, cut in half along the sagittal plane, and fixed in 4% paraformaldehyde for 24 h at 4 °C. Tissue was washed three times with PBS for 1 h at room temperature then embedded in 4% agrose, and 250-µm sections were cut using a Pelco 101 vibratome. Sections were washed three times in PBS containing 1% Triton-x100 for 30 min with gentle rotation and then incubated for 1 h in blocking solution: PBS containing 1% Triton-x100 and 20% goat serum. Sections were then incubated for 3 days at 4 °C in anti-IBA1 (Wako) and anti-β amyloid (already conjugated to AF488, Biolegend) primary antibodies each at a dilution of 1/300 in blocking solution. Sections were then washed three times in blocking solution followed by three washes in PBS containing 1% Triton-x100. Sections were incubated overnight at 4 °C in anti-rabbit AF633 (Life Technologies) at a dilution of 1/200 in blocking solution. Finally, sections were washed three times in PBS containing 1% Triton-x100. Prior to imaging, sections were cleared using RapiClear 1.49 by immersion in the clearing solution for 20 min at room temperature. The cleared tissues were then mounted on a custom-made sample holder and imaged using an Olympus FV1000 microscope. Images were processed with Amira 3D software.

Human. Brain paraffin-embedded slides were obtained from the Massachusetts Alzheimers Disease Research Center Brain Bank, and anti-IL-3 (1:100, 524379, US Biological), anti-IL-3Rα (1:50, 14-1239-82, 6H6, Thermo Fisher Scientific), Alex Fluor 488 anti-GFAP (1:50, 53-9892-82, GA5, Thermo Fisher Scientific), and anti-IBA1 (1:200, 019-19741, FUJIFILM Wako Chemicals) were used as primary antibodies. Biotinylated goat anti-rabbit IgG and horse anti-mouse IgG secondary antibodies were applied for IL-3 and IL-3Rα, respectively (1:100, BA-1000 and BA-2000, Vector Laboratories) followed by streptavidin DyLight 594 (1:600, SA-5594, Vector Laboratories). A goat anti-rabbit IgG secondary antibody, Alexa Fluor 488 (1:100, A-11034, Thermo Fisher Scientific) was used for IBA1 detection, and nuclei were counterstained with DAPI (1:3,000, D21490, Thermo Fisher Scientific). All the slides were scanned using a digital scanner NanoZoomer 2.0RS (Hamamatsu, Japan).

Microglia density and spatial analysis

During a preprocessing stage, the quality of the images was improved by reducing the fluorescence bleed-through signal and increasing the signal contrast to optimize cellular segmentation. To enhance cell contrast we used a contrast-limited adaptive histogram equalization algorithm and spatially filtered and denoised the images. A watershed algorithm was implemented to count individual cells, and a threshold was determined to reject objects with an area less than 45 μm^2. The centre position was determined for each cell. For each individual fluorescence channel, all processing and threshold parameters were kept fixed across all samples to guarantee consistency in the segmentation process of both Aβ plaques and microglia. The spatial data analysis was performed in 2D on the obtained segmented cells using a KNN (k-nearest neighbour) algorithm from the scikit-learn python package. For each segmented Aβ plaque, we then calculated the total number of microglia present at different interval distances from the centre of it. Specifically, we selected a fixed binning interval of 45 μm and incrementally calculated the number of microglia present in the circular area centred on the Aβ plaque and in the ring-shaped regions bounded by the concentric circles of progressively incrementing radii. The number of counted microglia was then normalized by the area of the considered region divided by the total number of microglia present in the brain section, and the average microglia density was then plotted as a function of distance. All software was written in python using opencv, numpy, and scikit-learn packages.

Molecular biology

Enzyme-linked immunosorbent assay. For mice, IL-3 levels were measured using an enzyme-linked immunosorbent assay (ELISA) kit (Boster Biological) according to the manufacturer's instructions. Three hours before they were killed, mice were injected with a biotinylated anti-IL-3 capture antibody (Biolegend) as previously described[28]. Measurement of Aβ was done as previously described[38]. In brief, brains were extracted and cortices were dissected and homogenized in 8 volumes of TBS containing 5 mM EDTA, phosphatase inhibitor (ThermoFisher), EDT-free protease inhibitor cocktail (Roche) and 2 mM 1,10-phenantroline (Sigma). Homogenates were centrifuged at 100,000g for 1 h at 4 °C using an Optima TL ultracentrifuge and a Ti70 rotor (Beckman Coulter). Supernatants were collected and used to measure TBS-soluble Aβ. The resulting pellet was homogenized in 70% formic acid. Samples were centrifuged at 100,000g for 1 h at 4 °C and supernatants were collected. FA-containing supernatants were neutralized with 1 M Tris-base, pH 11 (1:20 v-v) and samples were used to measure FA-soluble Aβ. Aβ40 and Aβ42 ELISAs were performed using Aβ ELISA kits (Wako).

Human brain IL-3 levels were measured using ELISA (Boster Biological). In brief, samples of human cortex were weighed, homogenized in RIPA buffer and centrifuged at 8,000 rpm for 2 min. IL-3 levels were measured in supernatant. Measurement of Aβ was done as previously described[38]. In brief, brains were extracted and cortices were dissected

and homogenized in 8 volumes of TBS containing 5 mM EDTA, phosphatase inhibitor (ThermoFisher), EDT-free protease inhibitor cocktail (Roche) and 2 mM 1,10-phenantroline (Sigma). Homogenates were centrifuged at 100,000g for 1 h at 4 °C using an Optima TL ultracentrifuge and a Ti70 rotor (Beckman Coulter). Supernatants were collected and used to measure TBS-soluble Aβ. The resulting pellet was homogenized in 70% FA. Samples were centrifuged at 100,000g for 1 h at 4 °C and supernatants were collected. FA-containing supernatants were neutralized with 1 M Tris-base, pH 11 (1:20 v-v) and samples were used to measure FA-soluble Aβ. Aβ40 and Aβ42 ELISAs were performed using Aβ ELISA kits (Wako).

Mouse qPCR. Total RNA was isolated using the RNeasy Mini Kit (Qiagen) or the NucleoSpin RNA XS kit (Takara Bio) according to the manufacturer's instructions. RNase-free DNase Set (Qiagen) was used for DNase digestion during RNA purification. RNA quantity and quality were assessed by Nanodrop for RNA isolated from tissues and with the Aglient RNA 6000 Pico kit (Aglient Technologies) on the Aglient 2100 Bioanalyzer for RNA of fluorescence-activated cell sorting (FACS)-purified cells. cDNA was generated from 1 μg total RNA per sample using the High Capacity cDNA Reverse Transcription Kit (Applied Biosystems). Quantitative real-time TaqMan PCR was performed using the following FAM-labelled TaqMan primers (Applied Biosystems): *Il3* (Mm00439631_m1), *Il3ra* (Mm00434273_m1), *Ccl2* (Mm00441242_m1), *C3* (Mm01232779_m1), *Gfap* (Mm01253033_m1), *Ccl7* (Mm00443113_m1), *Ccl5* (Mm01302427_m1), *Il1b* (Mm00434228_m1), *Tnfa* (Mm00443258_m1), *Il6* (Mm00446190_m1), *Il10* (Mm01288386_m1), *Ccl12* (Mm01617100_m1), *Trem2* (Mm04209424_g1), *Syk* (Mm01333032_m1), *Tyrobp* (Mm00449152_m1), *Cd33* (Mm00491152_m1), *Cd36* (Mm00432403_m1), *Tlr4* (Mm00445273_m1), *Sra* (Mm00491755_m1), *Cd206* (Mm01329362_m1), *Mpp9* (Mm00442991_m1), *Spp1* (Mm00436767_m1), *Clec7a* (Mm01183349_m1), *Lyz2* (Mm04214174_uH), *Apoe* (Mm01307192_m1), *Itgax* (Mm00498708_g1), *Itgam* (Mm00434455_m1), *Ptprc* (Mm01293577_m1), *Ctsg* (Mm00456011_m1), *Igf1* (Mm00439560), *Cd68* (Mm03047343_m1). VIC-labelled *Actb* (Mm00607939_s1) was used as the housekeeping gene. Results were analysed by the comparative CT method. Average CT values for each sample were normalized to the average CT values of the housekeeping gene.

Human qPCR. RNA was extracted from human brain tissue (frontal cortex) with Trizol (Life Technologies) according to the manufacturer's instructions. The extracted RNA was dissolved in water and purified using the RNAeasy Mini Kit (Qiagen) according to the manufacturer's protocol. Alternatively, RNA was isolated using E.Z.N.A. Total RNA kit (Omega Blotek). Purified RNA was quantified using Qubit RNA Broad Range Assay Kit (Thermo Fisher Scientific) on the Qubit Fluorometer 3.0 (Thermo Fisher Scientific). RNA (1 μg) was reverse-transcribed using the SuperScript III First Strand Synthesis System and oligo-DT(20) primer (Invitrogen). Gene expression was assessed by performing Taqman real-time PCR assays. The probe targeting human *Il3ra* was labelled with FAM (Hs00608141_m1, Thermo Fisher Scientific). The probe targeting the human housekeeping gene *Gapdh* was labelled with VIC (Hs02786624_g1, Thermo Fisher Scientific). 1:10 diluted cDNAs were mixed with the probes and Taqman Universal Master Mix II (Applied Biosystems) and amplified using the C1000 Touch Thermal Cycler (Bio-Rad). Results were analysed by the comparative CT method. Average CT values for each sample were normalized to the average CT values of the housekeeping gene. SNP genotyping was performed at two SNPs, rs429358 and rs7412, using a Taqman genotyping assay (Life Technologies) according to the manufacturer's instructions.

Behaviour phenotyping

Y-maze. Y-maze testing was adapted from published protocols[39]. The Y-maze apparatus consisted of three arms joined in the middle to form a Y shape. The walls of the arms were 10 cm high and each was marked with

Article

a single large black letter to serve as a spatial landmark and clue. With one arm of the maze closed, mice were allowed to explore the other two arms for 5 min before being returned to their home cage. Twenty minutes later, mice were returned to the Y-maze and allowed to explore all three arms for 5 min while being video recorded. The time spent in the new arm was quantified.

Morris water maze. The Morris water maze test was conducted in the Animal Behaviour Facility at the Massachusetts General Hospital. The Morris water maze test was performed with minor adjustments as previously described[40]. Spatial memory testing was conducted in a circular tank (diameter 1.22 m) filled with opacified water at 23 °C. The water tank was dimly lit and surrounded by a white curtain. The maze was virtually divided into four quadrants, with one containing a hidden platform (diameter 10 cm) that was submerged 0.5 cm below the water level. Four prominent cues were placed outside the maze as spatial references. Mice were placed in the water facing the tank wall at different start positions across trials in a quasi-random fashion to prevent strategy learning. Mice were allowed to search for the platform for 1 min; if the mice did not find the platform, they were guided towards it where they remained for 20 s. Each mouse went through four trials (one from each start position) per day for seven consecutive days. After each trial, the mouse was dried and placed back into its cage until the start of the next trial. All mouse movements were recorded by the computerized tracking system EthoVision XT (Noldus), which calculated distances moved and time required to reach the platform (escape latency), along with swim speed. The spatial probe trial was conducted 24 h after the last training session (on day 8). For the probe trial, the platform was removed and mice were allowed to swim for 1 min. The time spent by the mice in the area surrounding the location where the platform used to be (platform plus) was recorded. The platform plus surrounding the target is larger than the target itself, but smaller than the target quadrant. Data were calculated as time in the platform plus/60 s × 100% and is given as a percentage.

Illustrations

All illustrations were generated with a license to Biorender (https://www.biorender.com).

Statistics and reproducibility

Results are shown as mean ± s.e.m. Statistical analysis was performed using GraphPad Prism 7 (Graphpad Software). Statistical tests included unpaired, two-tailed non-parametric Mann–Whitney U-tests (when Gaussian distribution was not assumed). For multiple comparisons, a non-parametric multiple-comparisons test comparing the mean rank of each group (when Gaussian distribution was not assumed) was used, or one- or two-way ANOVAs followed by Tukey's test were used. For correlation analysis, the mean expression level from individuals of equal disease duration was determined and correlation was computed using Pearson correlation coefficients. P values of 0.05 or less were considered to denote significance. Each experiment was repeated independently at least three times with similar results.

Reporting summary

Further information on research design is available in the Nature Research Reporting Summary linked to this paper.

Data availability

RNA-seq data for microglia from *Il3*^{−/−}*5xFAD* and *5xFAD* mice have been deposited to NCBI-GEO under accession GSE163289. RNA-seq data for WT, *5xFAD*, *Trem2*^{−/−} and *Trem2*^{−/−}*5xFAD* mice have been previously described[24] and were deposited to GEO: GSE132508. scRNA sequencing data for homeostatic, DAM stage 1, and DAM stage 2 microglia have been previously described[23] and were deposited to GEO: GSE98969. Source data are provided with this paper.

27. Oakley, H. et al. Intraneuronal β-amyloid aggregates, neurodegeneration, and neuron loss in transgenic mice with five familial Alzheimer's disease mutations: potential factors in amyloid plaque formation. *J. Neurosci.* **26**, 10129–10140 (2006).
28. Weber, G. F. et al. Interleukin-3 amplifies acute inflammation and is a potential therapeutic target in sepsis. *Science* **347**, 1260–1265 (2015).
29. Turnbull, I. R. et al. Cutting edge: TREM-2 attenuates macrophage activation. *J. Immunol.* **177**, 3520–3524 (2006).
30. Doench, J. G. et al. Optimized sgRNA design to maximize activity and minimize off-target effects of CRISPR-Cas9. *Nat. Biotechnol.* **34**, 184–191 (2016).
31. Bae, S., Park, J. & Kim, J. S. Cas-OFFinder: a fast and versatile algorithm that searches for potential off-target sites of Cas9 RNA-guided endonucleases. *Bioinformatics* **30**, 1473–1475 (2014).
32. Hsiau, T. et al. Inference of CRISPR edits from Sanger trace data. Preprint at https://doi.org/10.1101/251082 (2018).
33. Kleinstiver, B. P. et al. Engineered CRISPR-Cas12a variants with increased activities and improved targeting ranges for gene, epigenetic and base editing. *Nat. Biotechnol.* **37**, 276–282 (2019).
34. Rohland, N. & Reich, D. Cost-effective, high-throughput DNA sequencing libraries for multiplexed target capture. *Genome Res.* **22**, 939–946 (2012).
35. Robbins, C. S. et al. Local proliferation dominates lesional macrophage accumulation in atherosclerosis. *Nat. Med.* **19**, 1166–1172 (2013).
36. DeVos, S. L. & Miller, T. M. Direct intraventricular delivery of drugs to the rodent central nervous system. *J. Vis. Exp.* **75**, e50326 (2013).
37. McQuade, A. et al. Development and validation of a simplified method to generate human microglia from pluripotent stem cells. *Mol. Neurodegener.* **13**, 67 (2018).
38. Griciuc, A. et al. Alzheimer's disease risk gene CD33 inhibits microglial uptake of amyloid beta. *Neuron* **78**, 631–643 (2013).
39. Kraeuter, A. K., Guest, P. C. & Sarnyai, Z. The Y-maze for assessment of spatial working and reference memory in mice. *Methods Mol. Biol.* **1916**, 105–111 (2019).
40. Vorhees, C. V. & Williams, M. T. Morris water maze: procedures for assessing spatial and related forms of learning and memory. *Nat. Protocols* **1**, 848–858 (2006).

Extended Data Fig. 1 | Analysis of *Il3*^{−/−} mice. a, FITC-dextran (mol. wt. 4000) was injected i.v. into WT and *Il3*^{−/−} mice before death. Blood–brain barrier integrity was determined by measuring the FITC signal in brain homogenate ($n = 6$ WT mice; $n = 4$ *Il3*^{−/−} mice). **b**, Before death, WT and *Il3*^{−/−} mice were injected i.v. with an anti-GR1 antibody conjugated to PE to label all circulating monocytes and neutrophils. PE signal among CD45⁺ cells was assessed in the brain by flow cytometry ($n = 7$ WT mice; $n = 4$ *Il3*^{−/−} mice). **c**, Doublecortin staining and quantification in the hippocampus of WT and *Il3*^{−/−} mice at 4 months of age ($n = 3$). **d**, Absence of caspase 3 staining in the hippocampus of WT and *Il3*^{−/−} mice along with a representative image of rare positively stained cells from the thalamus ($n = 3$). **e**, Assessment of MHCII⁺ microglia in the brains of WT and *Il3*^{−/−} mice ($n = 7$ WT mice; $n = 4$ *Il3*^{−/−} mice). **f**, Analysis of Ki67⁺ proliferating microglia ($n = 5$). **g**, Time in new arm during Y-maze testing ($n = 7$). Groups of mice are of evenly mixed sex. Mean ± s.e.m.
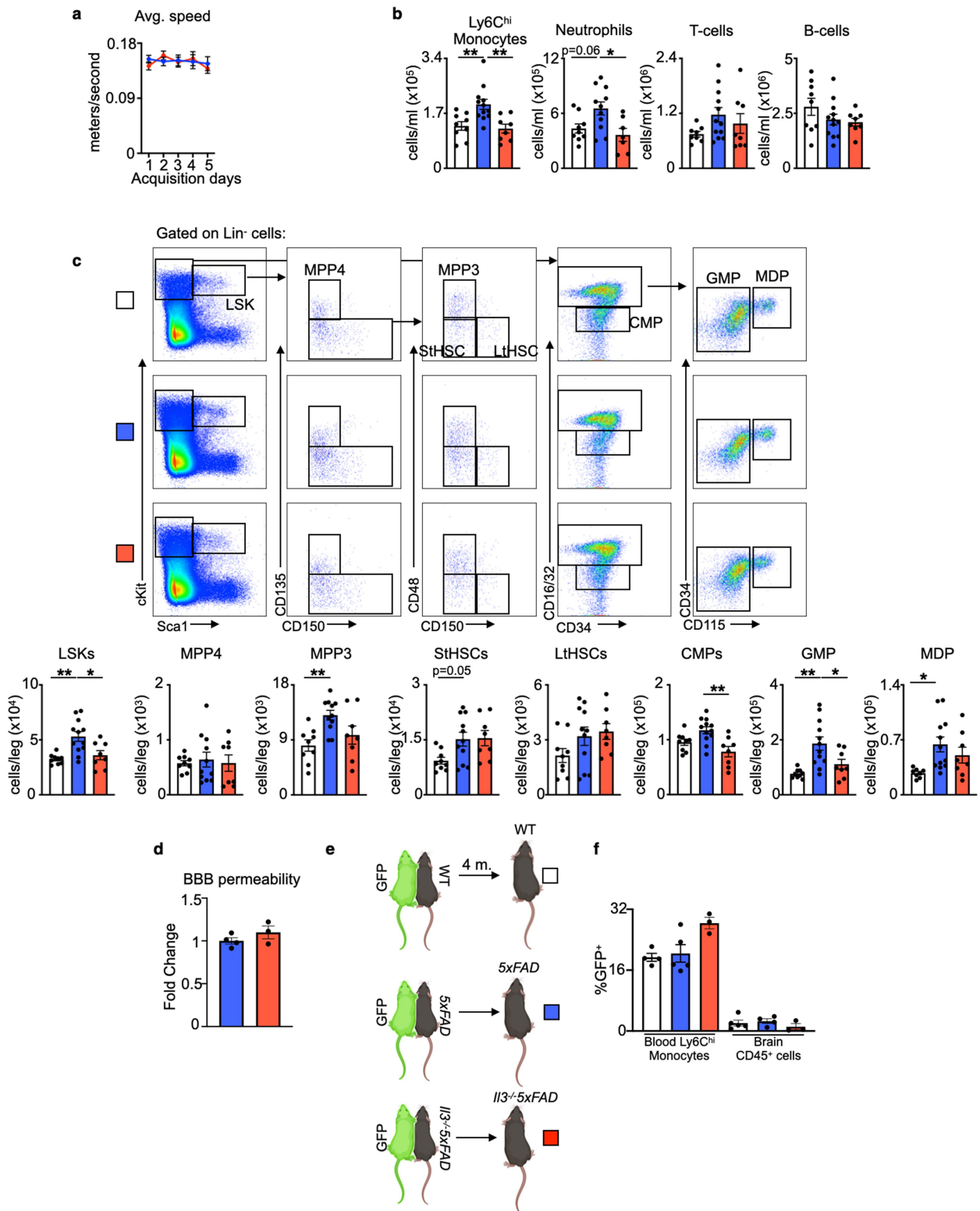
Extended Data Fig. 2 | Haematopoiesis and peripheral immune cell dynamics in WT, 5xFAD, and Il3$^{-/-}$5xFAD mice. a, Average swim speed during acquisition days of Morris water maze (n = 10 5xFAD mice; n = 9 Il3$^{-/-}$5xFAD mice). **b**, Flow cytometry assessment of blood leukocytes (n = 9 WT mice; n = 12 5xFAD mice; n = 8 Il3$^{-/-}$5xFAD mice). One-way ANOVA. **c**, Flow cytometry analysis of Lin$^-$SCA1$^+$cKIT$^+$ cells (LSKs), multi-potent progenitors (MPP)-4 and -3, short-term haematopoietic stem cells (StHSCs), long-term HSCs (LtHSCs), common myeloid progenitors (CMPs), granulocyte macrophage progenitors (GMPs), and monocyte dendritic progenitors (MDPs) in the bone marrow of 5-month-old WT, 5xFAD, and Il3$^{-/-}$5xFAD mice (n = 9 WT mice; n = 11 5xFAD mice; n = 8 Il3$^{-/-}$5xFAD mice). One-way ANOVA. **d**, FITC-dextran (mol. wt. 4,000) was injected i.v. into 5xFAD and Il3$^{-/-}$5xFAD mice before death. Blood–brain barrier integrity was determined by measuring the FITC signal in brain homogenates (n = 4). **e**, WT, 5xFAD, Il3$^{-/-}$5xFAD mice were joined by parabiosis with UbiGFP mice from the age of 2 to 6 months (4 months total). **f**, GFP chimerism in blood Ly6C^{hi} monocytes and brain CD45$^+$ cells was assessed by flow cytometry in the WT, 5xFAD, and Il3$^{-/-}$5xFAD parabionts (n = 4 WT mice; n = 5 5xFAD mice; n = 3 Il3$^{-/-}$5xFAD mice). Groups of mice are of evenly mixed sex. *P < 0.05, **P < 0.01, ***P < 0.001. Mean ± s.e.m.
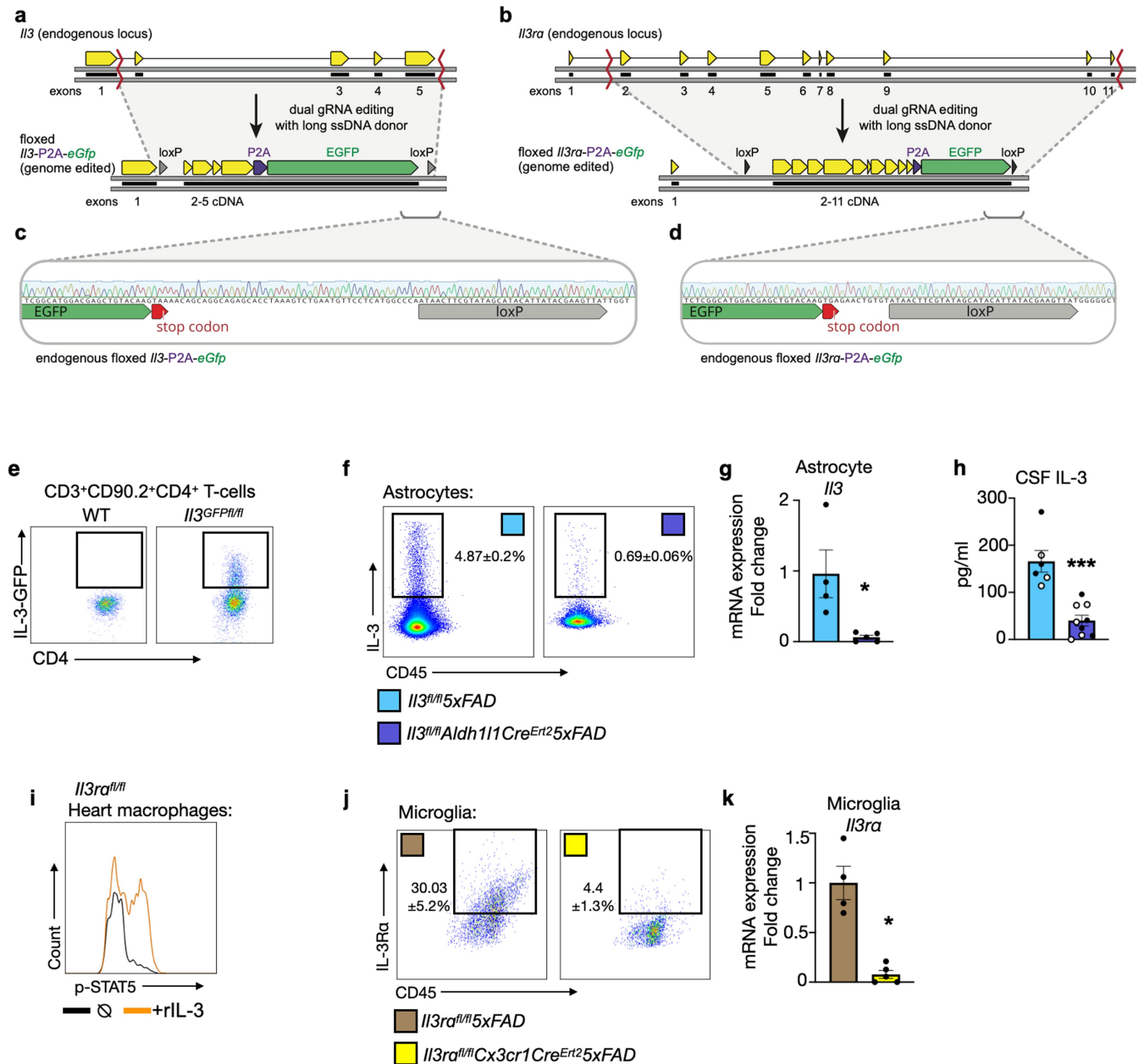
**Extended Data Fig. 3 | Generation and validation of *Il3^GFPfl/fl^Aldh1l1Cre^ERT2^ 5xFAD* and *Il3ra^fl/fl^Cx3cr1Cre^ERT2^5xFAD* mice. a**, **b**, Schematics of the endogenous loci and editing strategies to generate conditional/reporter models for *Il3* (**a**) and *Il3ra* (**b**). Mice were generated by excising large fragments of the endogenous loci by co-delivery of SpCas9 and two gRNAs, and in the presence of a long single-stranded DNA donor encoding a loxP-cDNA-P2A-EGFP-loxP cassette. **c**, **d**, Representative Sanger sequencing traces validating insertion of the loxP-cDNA-P2A-EGFP-loxP cassettes at the endogenous loci of *Il3* (**c**) and *Il3ra* (**d**). Missense mutation quenches the GFP signal in *Il3ra*-targeted mice. **e**, GFP signal in ex vivo-stimulated splenic and lymph node T cells, known IL-3 sources, from WT and *Il3^GFPfl/fl^* mice. **f**, Flow cytometry analysis of astrocyte IL-3 production in 5-month-old *Il3^GFPfl/fl^5xFAD* and *Il3^GFPfl/fl^*

Aldh1l1Cre^ERT2^5xFAD mice injected with tamoxifen. **g**, qPCR analysis of *Il3* mRNA expression in sorted astrocytes (n = 4 *Il3^GFPfl/fl^5xFAD* mice; n = 5 *Il3^GFPfl/fl^ Aldh1l1Cre^ERT2^5xFAD* mice). **h**, CSF IL-3 levels. Filled circles, males; open circles, females (n = 6 *Il3^GFPfl/fl^5xFAD* mice; n = 9 *Il3^GFPfl/fl^Aldh1l1Cre^ERT2^5xFAD* mice). **i**, STAT5 phosphorylation in ex vivo heart macrophages from *Il3rα^fl/fl^* mice simulated with rIL-3. **j**, Flow cytometry analysis of microglia IL-3Rα production in 5-month-old *Il3rα^fl/fl^5xFAD* and *Il3rα^fl/fl^Cx3cr1Cre^ERT2^5xFAD* mice injected with tamoxifen. **k**, qPCR analysis of *Il3rα* mRNA expression in sorted microglia (n = 4 *Il3rα^fl/fl^5xFAD* mice; n = 5 *Il3rα^fl/fl^Cx3cr1Cre^ERT2^5xFAD* mice). All *Il3^GFPfl/fl^5xFAD*, *Il3^GFPfl/fl^Aldh1l1Cre^ERT2^5xFAD*, *Il3rα^fl/fl^5xFAD*, and *Il3rα^fl/fl^Cx3cr1Cre^ERT2^ 5xFAD* mice were injected with tamoxifen beginning at 2 months of age. **P < 0.01, ***P < 0.001, two-tailed Mann–Whitney U-tests. Mean ± s.e.m.
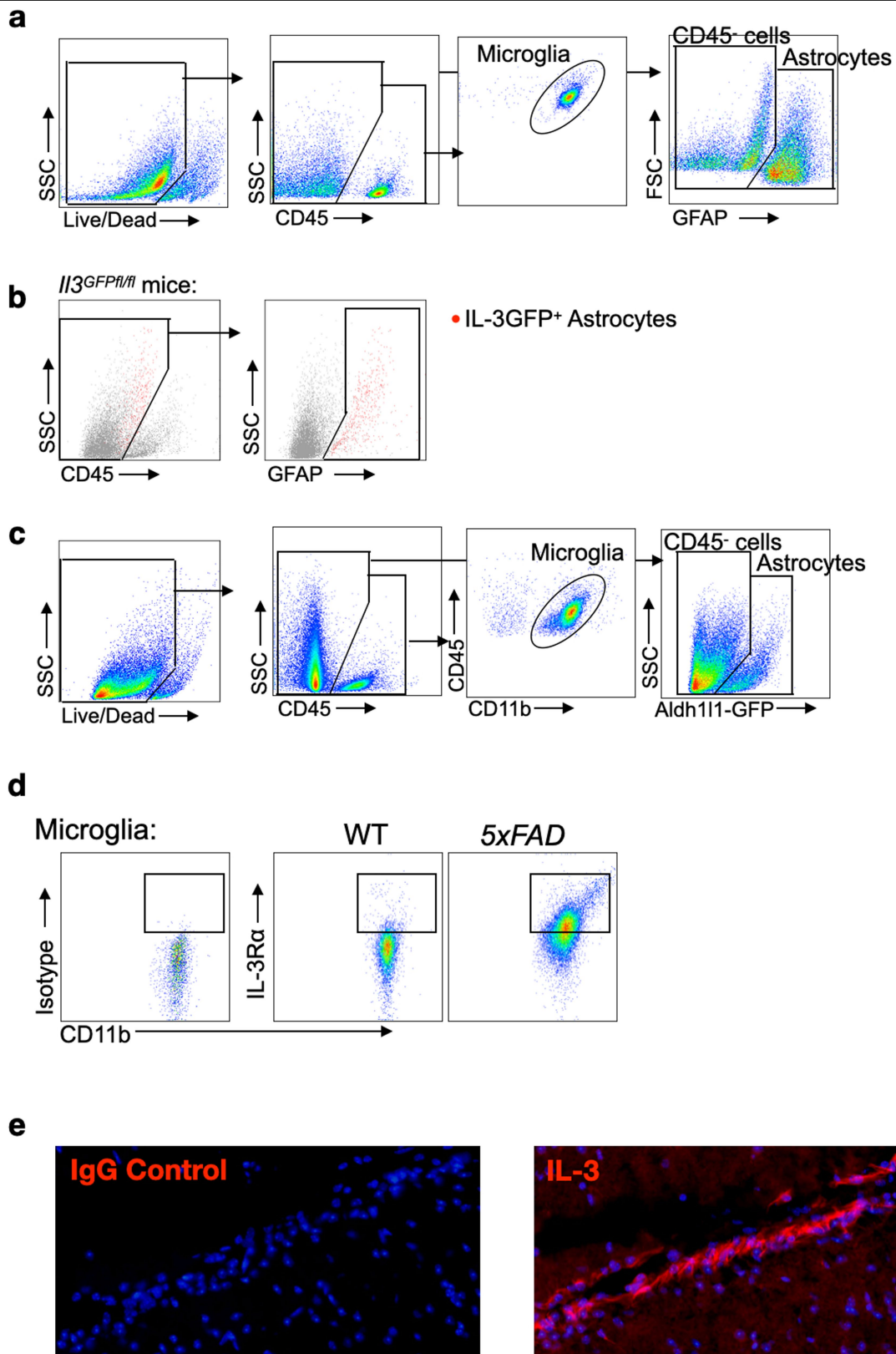
**Extended Data Fig. 4 | Flow cytometry gating strategy and histology controls. a**, Gating strategy used to identify cell populations in the brains of all mice except *Aldh1l1^GFP* mice. **b**, Backgating of GFP⁺ astrocytes in *Il3^GFPfl/fl* mice. **c**, Gating strategy used to identify cell populations in the brain of *Aldh1l1^GFP* mice. **d**, Gating and isotype control plots for microglia IL-3Rα staining. **e**, Representative images of IgG control antibody staining and IL-3 staining in the brain.

Article
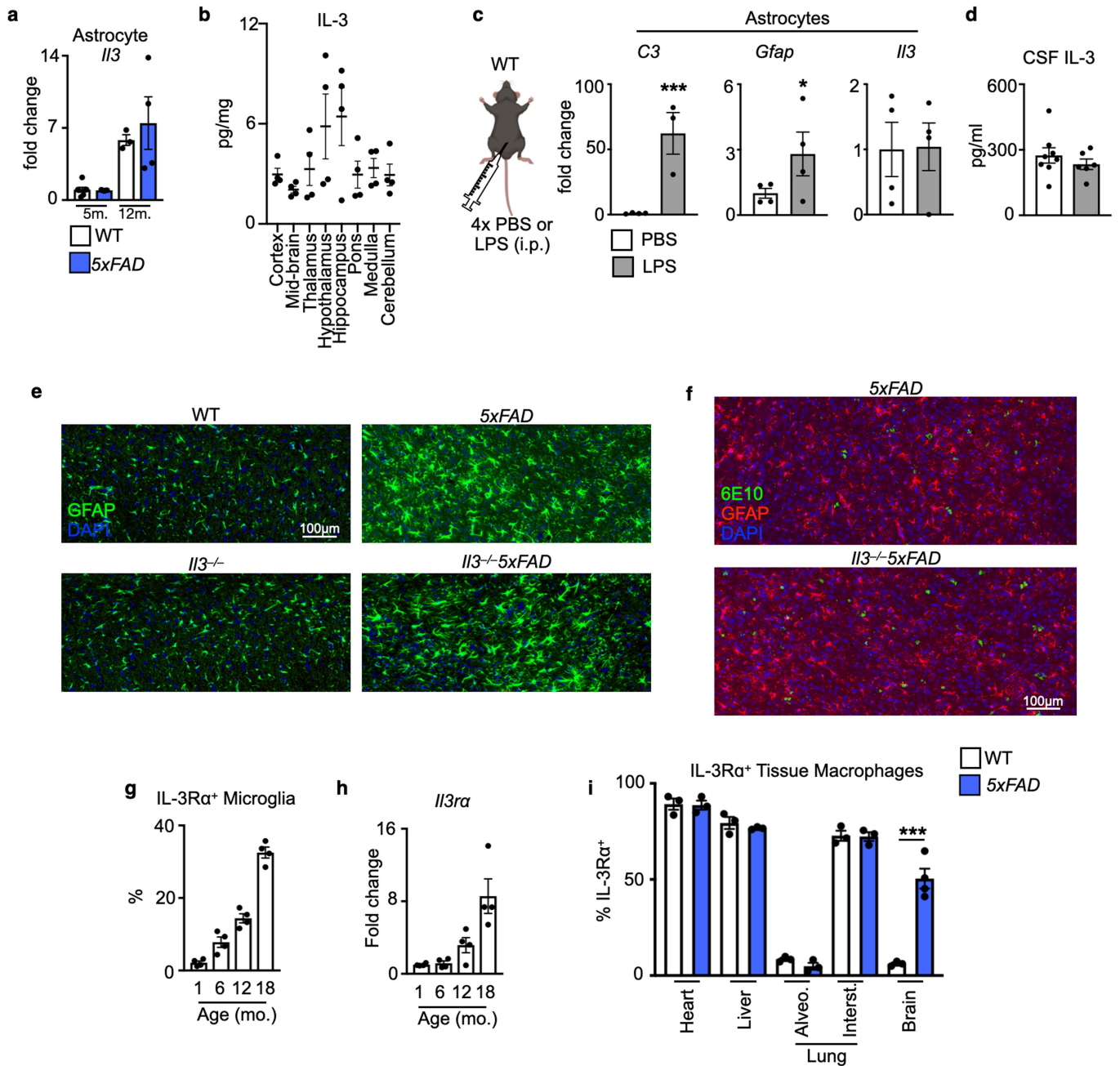
Extended Data Fig. 5 | Astrocyte IL-3 and microglia IL-3Rα production. a, *Il3* expression in astrocytes sorted from WT and *5xFAD* mice at 5 and 12 months of age (*n* = 5 5-month-old WT mice; *n* = 4 5-month-old *5xFAD* mice; *n* = 3 12-month-old WT mice; *n* = 4 12-month-old *5xFAD* mice). **b**, Tissue IL-3 levels in various brain regions in WT mice at 4 months of age (*n* = 4). **c**, Scheme of daily i.p. LPS injection into WT mice over 4 days and qPCR analysis of *C3* and *Gfap* in sorted astrocytes after LPS injection (*n* = 4 PBS mice; *n* = 3 LPS mice for *C3*; *n* = 4 LPS mice for *Gfap* and *Il3*). Two-tailed Mann–Whitney *U*-tests. **d**, CSF IL-3 levels (*n* = 8 WT PBS mice; *n* = 6 LPS mice). **e**, Representative images of GFAP+

astrocytes in the cortex of WT, *Il3⁻/⁻*, *5xFAD*, and *Il3⁻/⁻5xFAD* mice. **f**, Representative images of Aβ deposits (6E10) and astrocytes (GFAP) in *5xFAD* and *Il3⁻/⁻5xFAD* mice. **g**, Proportion of IL-3Rα+ microglia in the brain of WT mice at various ages (*n* = 4). **h**, *Il3ra* transcript expression in brain homogenate from WT mice at various ages (*n* = 4). **i**, Proportion of IL-3Rα+ macrophages in heart, liver, lung (interstitial and alveolar), and brain of WT and *5xFAD* mice at 8 months of age (*n* = 3 WT and *5xFAD* mice for all tissues except brain where *n* = 4). One-way ANOVA. *P < 0.05, **P < 0.001. Mean ± s.e.m.

a Microglia scRNA-seq; Keren-Shaul *et. al. Cell*, 2017
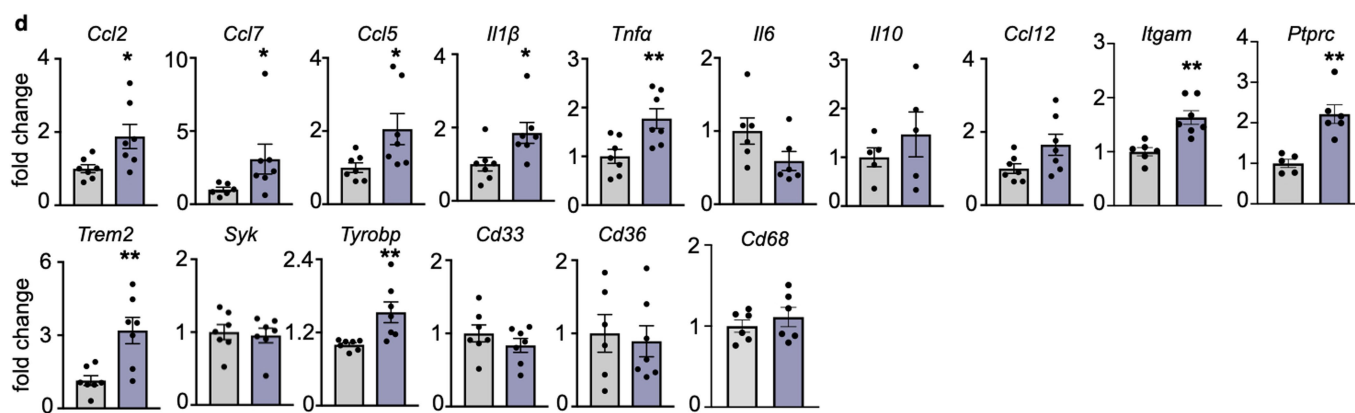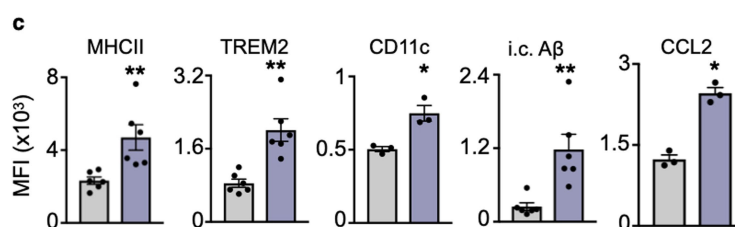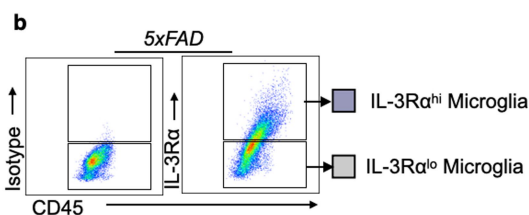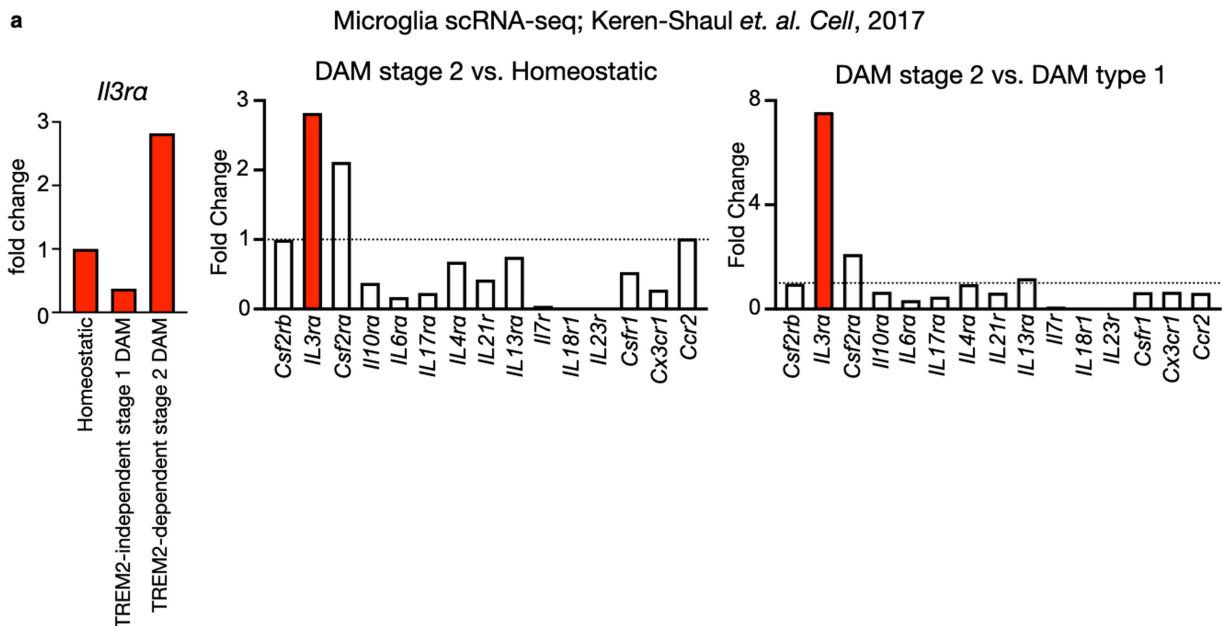
Extended Data Fig. 6 | *Il3ra* expression in microglia and characterization of IL-3Rα^hi and IL-3Rα^lo microglia. a, Analysis of *Il3ra* and other cytokine receptors expressed in homeostatic, DAM stage 1, and DAM stage 2 microglia (data from ref.[23]). **b**, Gating strategy for IL-3Rα^hi and IL-3Rα^lo microglia from *5xFAD* mice. **c**, Flow cytometry analysis of IL-3Rα^hi and IL-3Rα^lo microglia (*n* = 6 except CD11c and CCL2 where *n* = 3). **d**, mRNA transcript expression in sorted IL-3Rα^hi and IL-3Rα^lo microglia (*n* = 7 for IL-3Rα^lo microglia except that *n* = 6 for *Il6*, *Itgam*, *Ptprc*, *Cd36*, and *Cd68*, and *n* = 5 for *Il10*; *n* = 7 for IL-3Rα^hi microglia except that *n* = 6 for *Il6*, *Ptprc* and *Cd68*, and *n* = 5 for *Il10*). *P < 0.05, **P < 0.01, two-tailed Mann–Whitney *U*-tests. Mean ± s.e.m.
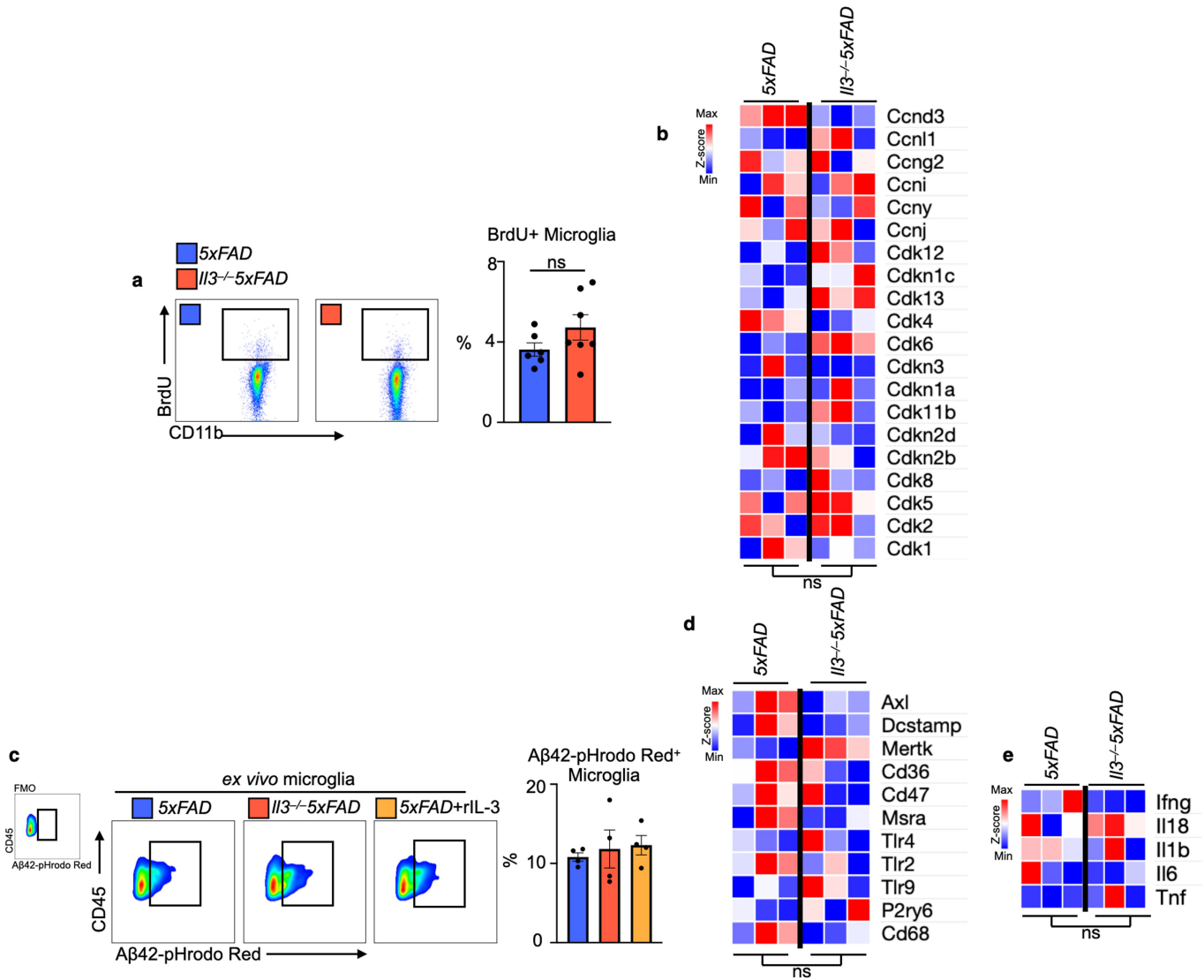
Extended Data Fig. 7 | IL-3 does not influence proliferation, recognition and phagocytosis of Aβ, or production of inflammatory cytokines in microglia. a, BrdU incorporation into microglia ($n = 6$ 5xFAD; $n = 7$ Il3⁻/⁻ 5xFAD). Two-tailed Mann–Whitney U-tests. **b**, Heat map of microglia RNA-seq expression data for genes important for cell cycle and proliferation. **c**, Assessment of ex vivo phagocytosis of Aβ42 conjugated to a pH-sensitive dye (PHrodo Red) in sorted microglia lacking Il3 or stimulated with rIL-3 ($n = 4$). **d**, Heat map of microglia RNA-seq expression data for genes important for Aβ recognition and phagocytosis. **e**, Heat map of microglia RNA-seq expression data for inflammatory cytokines. Groups of mice are of evenly mixed sex. Mean ± s.e.m.; ns, not significant.
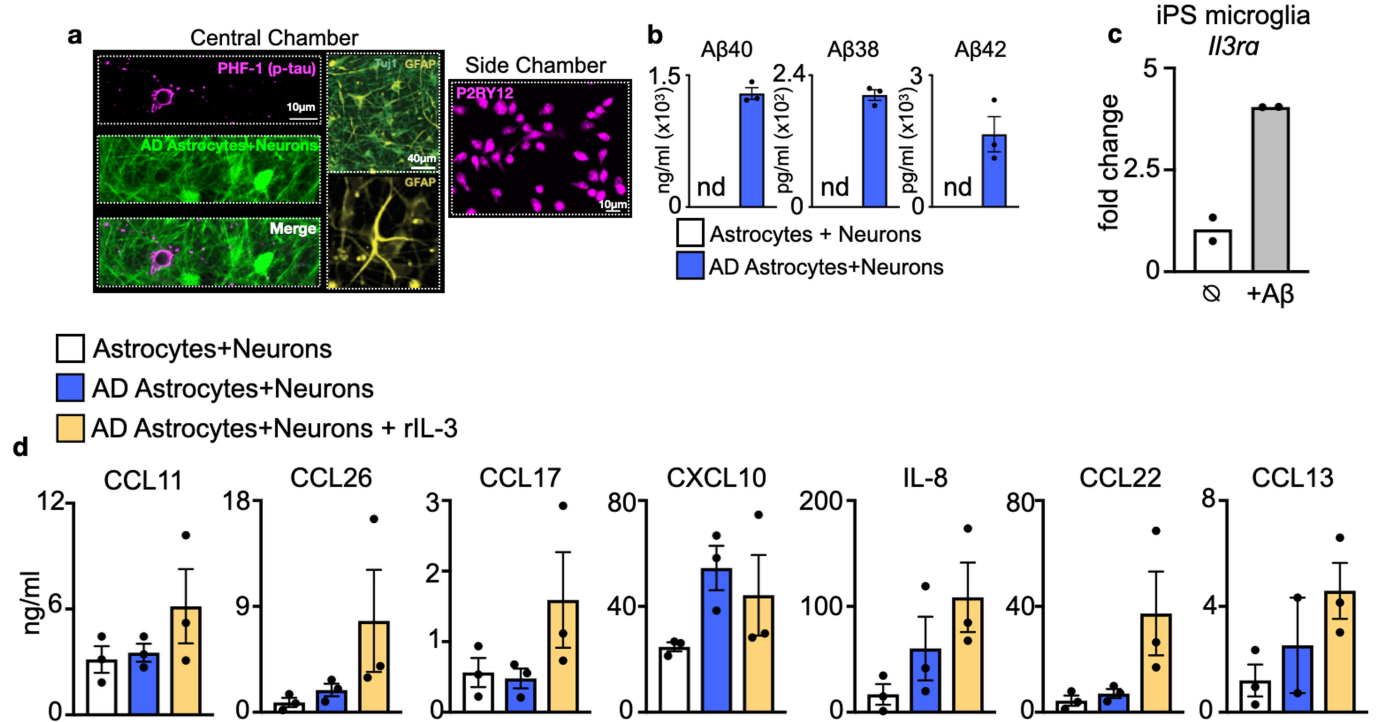
Extended Data Fig. 8 | Human AD iPS triculture system. a, Representative images demonstrating p-tau (PHF1) localization with neurons (TUJ1) and the presence of astrocytes (GFAP) in the central chamber, and microglia (P2RY12) in the side chamber. **b**, ELISA quantification of Aβ40, Aβ38, and Aβ42 in medium (n = 3 per group). **c**, *IL3RA* expression in human iPS microglia exposed to Aβ (n = 2). **d**, Chemokine and cytokine levels in the medium of the human AD iPS triculture system (n = 3 except n = 2 for CCL13 AD astrocytes + neurons). Mean ± s.e.m.
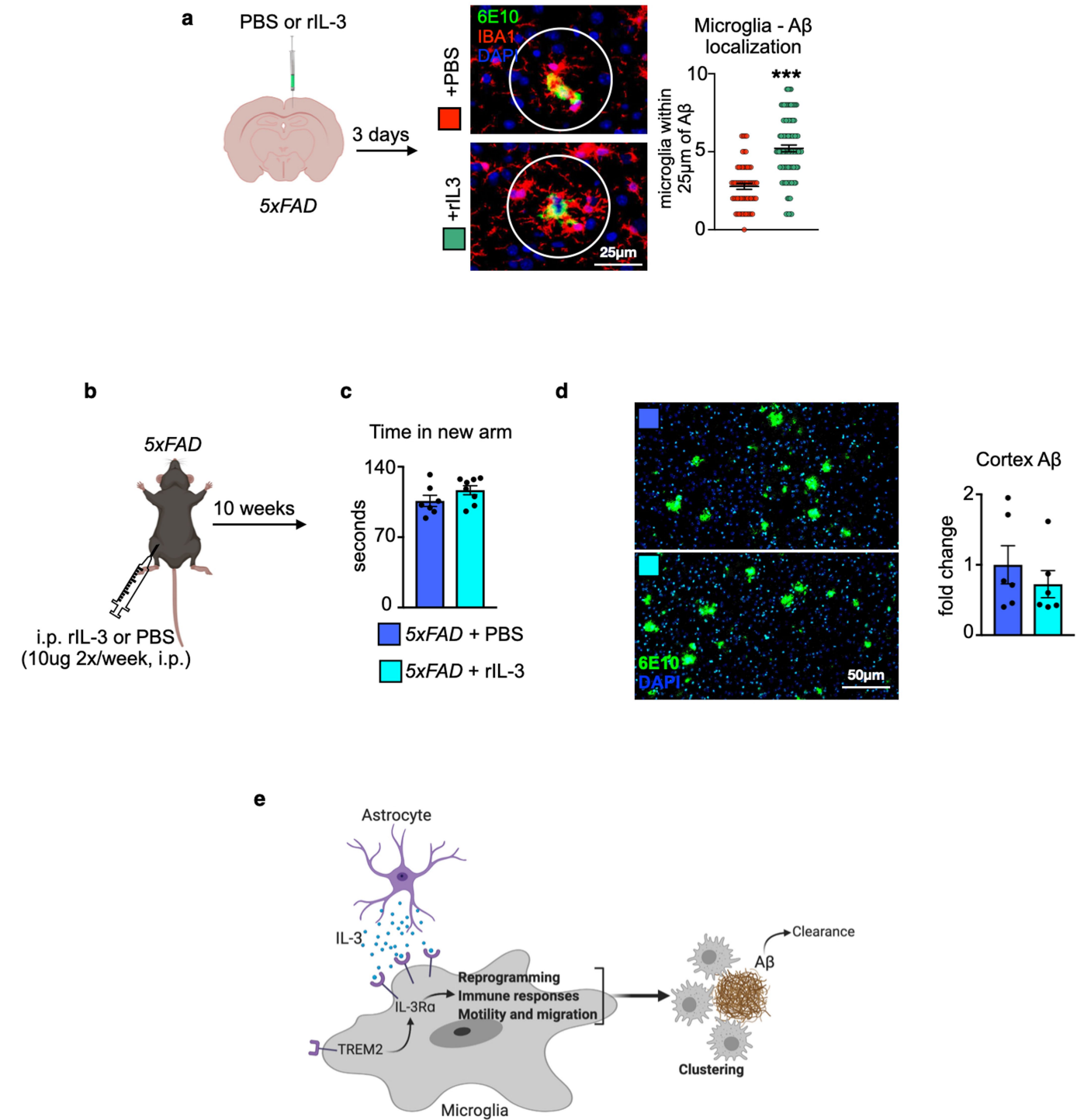
Extended Data Fig. 9 | rIL-3 delivery to the cortex or periphery of *5xFAD* mice and summary figure. a, Recombinant IL-3 or PBS was delivered into the cortex of *5xFAD* mice. Three days later, localization of microglia to Aβ aggregates was assessed (*n* = 7 PBS mice; *n* = 6 rIL-3 mice). Two-tailed Mann–Whitney *U*-tests. **b**, Scheme of rIL-3 delivery intraperitoneally twice a week for 10 weeks to *5xFAD* mice. **c**, Prior to death, Y-maze behavioural testing was performed and time in the new arm was quantified (*n* = 7 PBS mice; *n* = 8 rIL-3 mice). **d**, The amount of Aβ in the cortex of mice was quantified by analysing histological sections (*n* = 6). Groups of mice are of evenly mixed sex. **P < 0.01. Mean ± s.e.m. **e**, Model of the role of IL-3 in AD. Astrocytes produce IL-3. In response to Aβ, TREM2 signalling increases microglia IL-3Rα, rendering microglia responsive to astrocyte-derived IL-3. IL-3 signalling instigates transcriptional and functional programming of microglia, which leads to a signature of immune regulation, motility, and migration. IL-3-dependent programming promotes clustering of microglia around Aβ, which enables clearance of Aβ and mitigation of AD pathology.

Extended Data Table 1 | Characteristics of control donors and patients with AD

Characteristics of control and AD cases used for Fig. 3b, g, and h.			Characteristics of control and AD cases used for Fig. 3d-f		
Characteristics	**Controls (n=15)**	**AD (n=23)**	**Characteristics**	**Controls (n=28)**	**AD (n=30)**
Age at death (years)	83.33±10.28	74±2.06	Age at death (years)	81.44±7.44	78.57±10.73
Disease duration (min-max)	NA	9.4 (5-12)	Disease duration (min-max)	NA	10.7 (5-21)
Males/Females (%)	66.66/33.33	50/50	Males/Females (%)	50/50	35.7/64.3
			APOEε4 carriers	6 (3M/3F)	23 (9M/14F)
			APOEε4 homozygous carriers	0	11 (6M/5F)

nature research

Corresponding author(s): Rudolph Tanzi, Filip Swirski

Last updated by author(s): Jun 3, 2021

Reporting Summary

Nature Research wishes to improve the reproducibility of the work that we publish. This form provides structure for consistency and transparency in reporting. For further information on Nature Research policies, see our Editorial Policies and the Editorial Policy Checklist.

Statistics

For all statistical analyses, confirm that the following items are present in the figure legend, table legend, main text, or Methods section.

n/a	Confirmed	
☐	☒	The exact sample size (*n*) for each experimental group/condition, given as a discrete number and unit of measurement
☐	☒	A statement on whether measurements were taken from distinct samples or whether the same sample was measured repeatedly
☐	☒	The statistical test(s) used AND whether they are one- or two-sided *Only common tests should be described solely by name; describe more complex techniques in the Methods section.*
☐	☒	A description of all covariates tested
☐	☒	A description of any assumptions or corrections, such as tests of normality and adjustment for multiple comparisons
☐	☒	A full description of the statistical parameters including central tendency (e.g. means) or other basic estimates (e.g. regression coefficient) AND variation (e.g. standard deviation) or associated estimates of uncertainty (e.g. confidence intervals)
☐	☒	For null hypothesis testing, the test statistic (e.g. F, t, r) with confidence intervals, effect sizes, degrees of freedom and P value noted *Give P values as exact values whenever suitable.*
☒	☐	For Bayesian analysis, information on the choice of priors and Markov chain Monte Carlo settings
☒	☐	For hierarchical and complex designs, identification of the appropriate level for tests and full reporting of outcomes
☐	☒	Estimates of effect sizes (e.g. Cohen's *d*, Pearson's *r*), indicating how they were calculated

Our web collection on statistics for biologists contains articles on many of the points above.

Software and code

Policy information about availability of computer code

Data collection	Graphpad Prism 7.0a, DIVA, Amira, NPD.view, ImageJ, Applied Biosystems 7300, R package edgeR, i-Control Microplate Reader Software, EthoVision XT
Data analysis	Graphpad Prism 7.0a, Flowjo, Amira, ImageJ, Excel, NDP.view, Ensembl

For manuscripts utilizing custom algorithms or software that are central to the research but not yet described in published literature, software must be made available to editors and reviewers. We strongly encourage code deposition in a community repository (e.g. GitHub). See the Nature Research guidelines for submitting code & software for further information.

Data

Policy information about availability of data

All manuscripts must include a data availability statement. This statement should provide the following information, where applicable:
- Accession codes, unique identifiers, or web links for publicly available datasets
- A list of figures that have associated raw data
- A description of any restrictions on data availability

The authors declare that all data supporting the findings of this study are available within the paper, its supplementary information files, or publicly available. RNA sequencing data of microglia from Il3–/–5XFAD vs. 5XFAD mice has been deposited to NCBI-GEO: GSE163289 (will be shared upon request and will be made publicly available at time of publication). RNA sequencing data of WT vs. 5XFAD vs. Trem2–/- vs. Trem2–/–5XFAD has been previously described and was deposited to NCBI-GEO: GSE132508. scRNA sequencing data of homeostatic, DAM stage 1, and DAM stage 2 microglia has been previously described and was deposited to GEO: GSE98969.

Field-specific reporting

Please select the one below that is the best fit for your research. If you are not sure, read the appropriate sections before making your selection.

☒ Life sciences   ☐ Behavioural & social sciences   ☐ Ecological, evolutionary & environmental sciences

For a reference copy of the document with all sections, see nature.com/documents/nr-reporting-summary-flat.pdf

Life sciences study design

All studies must disclose on these points even when the disclosure is negative.

Sample size	Power calculations were conducted to determine sample size.
Data exclusions	No data were excluded from the analysis
Replication	All experiments were successfully repeated at least 3 times using separate cohorts
Randomization	Where appropriate, the mice were selected at random. Otherwise, animals were placed into separate groups according to their genotype. Humans were placed in control or AD groups according to clinical diagnosis as described in the methods section
Blinding	All experiments were blinded.

Reporting for specific materials, systems and methods

We require information from authors about some types of materials, experimental systems and methods used in many studies. Here, indicate whether each material, system or method listed is relevant to your study. If you are not sure if a list item applies to your research, read the appropriate section before selecting a response.

Materials & experimental systems

n/a	Involved in the study
☐	☒ Antibodies
☐	☒ Eukaryotic cell lines
☒	☐ Palaeontology and archaeology
☐	☒ Animals and other organisms
☐	☒ Human research participants
☒	☐ Clinical data
☒	☐ Dual use research of concern

Methods

n/a	Involved in the study
☒	☐ ChIP-seq
☐	☒ Flow cytometry
☒	☐ MRI-based neuroimaging

Antibodies

Antibodies used: anti-CD45 (BioLegend, clone30-F11, cat103147, lotB294297), anti-CD3 (BioLegend, clone 17A2, cat100206, lotB263030), anti-CD90.2 (BioLegend, clone 53-2.1, catc, lotBs60050), anti-CD19 (BioLegend, clone 6D5, cat115508, lotB273503), anti-B220 (BD Biosciences, clone RA3-6B2, cat553089, lotB250169), anti-NK1.1 (BioLegend, clone PK136, cat108708, lotB296414), anti-Ly-6G (BioLegend, clone 1A8, cat127614, lotB258704), anti-Ly-6C (BioLegend, AL-21, cat128006, lotB270133), anti-MHCII (BioLegend, clone M5/114.152, cat107602, lotB303311), anti-CD11b (BioLegend, clone M1/70, cat101226, lotB281906), anti-CD115 (BioLegend, clone AFS98, cat135517, lotB301974), anti-Ter119 (BioLegend, clone TER- 119, cat116208, lotB290995), anti-CD34 (eBioscience, clone RAM34, cat11-0341-85, lot2112197), anti-CD49b (BioLegend, clone DX5, cat1089008, lotB258302), anti-CD11c (BioLegend, clone N418, cat117310, lotB275102), anti-IL-7Rα (BioLegend, clone SB/199, cat121112, lotED1471-1630), anti-CD16/32 (BioLegend, clone 93, cat101324, lotB250025), anti-CD150 (BioLegend, clone TC15-12F12.2, cat115922, lotB293276), anti-cKit (BioLegend, clone 2B8, cat105814, lotB285155), anti-CD135 (BioLegend, clone A2F10, cat135310, lotB193725), anti-CD48 (BioLegend, clone HM48-1, cat103426, lotB279067), anti- Sca1 (BioLegend, clone D7, cat108126, lotB283742), anti-IL-3 (BD Bioscience, clone MP2-8F8, cat55483, lot0022115), anti-IL-3Rα (eBioscience, clone 6H6, cat14-1239-82, lot5181120068), anti-GFAP (eBioscience, G5A, cat53-982-80, lot2068179), anti CCL2 (eBioscience, clone 2H5, cat11-7096-81, lot2634119), anti-β-amyloid (BioLegend, clone 6E10, cat803013, lotB307268), anti-TREM2 (R&D Systems, clone 237920, catFAB17291P, lotAADX0616121), anti-BrdU (eBioscience, clone BU20A, cat17-5071-42, lot2045491). anti-PHF (A gift from P. Davies, Albert Einstein College of Medicine), anti-GFAP (Millipore, AB5804), anti-P2RY12 (Sigma, HPA013796), anti-IL3ra (Biolegend, 306004), anti-beta-tubulin III (Abcam, ab18207), anti-IL3 (Invitrogen, CF500182). Anti-Iba1 (Fujifilm Wako, 019-19741), streptavidin DyLight 594 (Vector Laboratories, BA- 1000, SA-5594), anti-GFP (Abcam, ab13970), anti-chicken IgY secondary antibody, Alexa Fluor 488, Thermo Fisher Scientific, A-11039), anti-IL3 (Biolegend, MP2-8F8), anti-rat IgG secondary antibody (Vector Laboratories, SA-5594, BA-4001), anti-GFAP (Thermo Fisher Scientific, 42-9892-80, GA5), IL3ra (US biologicals, 141039), anti-Iba1 (Abcam, ab5076), anti-rabbit IgG secondary (Thermo Fisher Scientific, A-31572), anti-rabbit AF633 (Life Technologies, A-21070). Human anti-IL3 (US Biological, 524379), anti-IL-3Rα (14-1239-82, 6H6, Thermo Fisher Scientific), anti-GFAP (53-9892-82, GA5, Thermo Fisher Scientific), anti-rabbit IgG (Vector Laboratories, BA- 1000), anti-mouse IgG (Vector Laboratories, BA-2000), anti-rabbit IgG (Thermo Fisher Scientific, A-11034), AF488 anti-CD45 (Biolegend, 30-F11, cat103121)

Validation	These antibodies are all used in flow cytometry and have been validated by the corresponding companies. The validation materials can be found on the companies' website. The specificity and sensitivity of each antibody is thoroughly validated. This is done by staining multiple target cells with either single- or multi-color analysis or by other testing approaches. The QC specifications and testing SOPs and gold standard for each product are then developed. The functional performance of each batch of products is strictly QC-tested according to the established QC procedures.

Eukaryotic cell lines

Policy information about cell lines

Cell line source(s)	ReN cell VM human neural progenitor cells (NPCs): EMD millipore and NINDS iPSC cell repository distributed through RUCDR, www.rucdr.org
Authentication	Authentication and validation information can be found on the sources' website.
Mycoplasma contamination	Cell lines were not tested for mycoplasma contamination
Commonly misidentified lines (See ICLAC register)	no commonly misidentified cell lines were used in the study

Animals and other organisms

Policy information about studies involving animals; ARRIVE guidelines recommended for reporting animal research

Laboratory animals	Wild-type C57BL/6J, B6;FVB-Tg(Aldh1l1-EGFP/Rpl10a)JD130Htz/J, C57BL/6J-Trem2em2Adiuj/J, and C57BL/6-Tg(UBC-GFP)30Scha/J mice were purchased from The Jackson Laboratory. 5xFAD mice were purchased from the Jackson Laboratory (MMRRC) and backcrossed onto the C57BL/6J background more than 10 generations before being crossed with other strains. Il3–/– mice on the C57BL/6J background were bred in- house2,3 and crossed with 5xFAD mice. For RNAseq studies, Trem2–/– mice on the C57BL/6J background were generated at Washington University School of Medicine, bred in-house, and crossed with 5xFAD mice. Il3GFPfl/fl and Il3rafl/fl mice were generated in-house as described in the methods section. Female and male mice at 5, 8, and 12 months of age were use. The specific age and sex of the animals are indicated within each figure.
Wild animals	This study did not involve wild animals
Field-collected samples	This study did not involve field collected samples
Ethics oversight	All animal protocols were approved by the Animal Review Committee at the Massachusetts General Hospital (protocol no. 2011N000035 and 2015N000044) and were in compliance with relevant ethical regulations.

Note that full information on the approval of the study protocol must also be provided in the manuscript.

Human research participants

Policy information about studies involving human research participants

Population characteristics	Tissue from healthy control individuals and individuals diagnosed with AD were used. Detailed population characteristics including age, sex, diagnosis, and Apoe genotype are described in Extended Data Table 6 and Extended Data Table 7.
Recruitment	Frozen tissue specimens and paraffin sections from the frontal cortex of AD patients and age-matched non-demented control subjects were obtained from the Massachusetts Alzheimers Disease Research Center Brain Bank. Subjects or next of kin consented to the brain donation and the Massachusetts General Hospital Institutional Review Board approved the study. All AD patients met the National Institute of Neurological and Communicative Disorders and Stroke-Alzheimer's Disease and Related Disorders Associations criteria for probable AD and the National Institute on Aging-Reagan Institute criteria for high likelihood of AD. There were no self-selection bias or other biases in sample selection.
Ethics oversight	Secondary use of de-identified human samples was approved by the institutional review board of the Massachusetts General Hospital (protocol no. 2019P003736 and 2019P003732).

Note that full information on the approval of the study protocol must also be provided in the manuscript.

Flow Cytometry

Plots

Confirm that:

☐ The axis labels state the marker and fluorochrome used (e.g. CD4-FITC).

☐ The axis scales are clearly visible. Include numbers along axes only for bottom left plot of group (a 'group' is an analysis of identical markers).

☒ All plots are contour plots with outliers or pseudocolor plots.

☒ A numerical value for number of cells or percentage (with statistics) is provided.

Methodology

Sample preparation

Peripheral blood was collected by retro-orbital bleeding and red blood cells were lysed in RBC lysis buffer (Biolegend). Bone marrow cells were collected by flushing bones with PBS, after which a single-cell suspension was created by passing cells through a 26-gauge needle and red blood cells were lysed with RBC lysis buffer. Brain was excised after PBS (Thermo Fisher Scientific) perfusion, minced and digested with 450 U ml-1 collagenase I, 125 U ml−1 collagenase XI, 60 U ml−1 DNase I and 60 U ml−1 hyaluronidase (Sigma) in PBS for 40 min at 37 °C. Samples were passed through a 70-μm cell strainer and mixed with 30% percol layered on-top of 70% percol. The percol gradient was centrifuged at 500g for 30 mins with brake off. The cell fraction was collected and washed with PBS before downstream applications. Total viable cell numbers were counted using trypan blue (Cellgro, Mediatech) or counting beads (Thermo Fisher Scientific).

Instrument

LSRII and AriaII

Software

DIVA and Flowjo

Cell population abundance

Post sort, cell abundance was sufficient for down stream applications. After sorting, a small fraction of the sorted cells were run through Aria II and the same gating strategy was applied to check the purity of sorted cell populations. A general purity of higher than 95% were achieved for all the sorted population.

Gating strategy

FSC/SSC gating was used to exclude dead cells and debris followed by FSC-A/FSC-H to specify singlets. Zombie Aqua (BV510) or 7AAD were used to further gate out dead cells. Live, singlet cells were identified as (1) Ly-6Chigh monocytes (CD45+CD11b+CD115+Ly- 6Chigh), (2) neutrophils (CD45+CD11b+Ly-6G+), (3)Bcells(CD45+B220+CD19+CD11b−), (4) T cells (CD45+CD3+CD90+CD11b−), (5) LSK cells (CD45+Lin−Kit+Sca1+), (6) multipotent progenitor (MPP)4 (CD45+Lin−Kit+Sca1+CD135+CD150−), (7) MPP3 (CD45+Lin−Kit+Sca1+CD135+CD150−CD48+), (8) short-term hematopoietic stem cells (CD45+Lin−Kit+Sca1+CD135+CD150−CD48−), (9) long-term hematopoietic stem cells (CD45+Lin−Kit+Sca1+CD135+CD150+CD48−), (10) common myeloid progenitor (CD45+Lin−Kit+Sca1−CD34+CD16/32mid), (11) granulocyte–macrophage progenitor (CD45+Lin−Kit+Sca1−CD34+CD16/32highCD115−), (12) monocyte–dendritic cell progenitor (CD45+Lin−Kit+Sca1−CD34+CD16/32highCD115+), (13) Microglia (CD45midCD11b+), (14) Astrocytes (CD45- CD11b-GFAP+ or CD45-CD11b-Aldh1l1-GFP+), (15) Other brain cells (CD45-CD11b-GFAP- or CD45-CD11b- Aldh1l1-GFP-). Lin=B220, CD19, CD49b, Ter119, CD90.2, CD11b, CD11c, Ly6G, IL7Rα.

☒ Tick this box to confirm that a figure exemplifying the gating strategy is provided in the Supplementary Information.